https://doi.org/10.1016/j.compstruct.2024.118088

Mechanistic model for the compression strength prediction of masonry columns strengthened with fibre-polymer composites

Luis C.M. da Silva[a,*], Gabriele Milani[a], Ernesto Grande[b], Marco F. Funari[c]

[a] *Department A.B.C., Politecnico di Milano, Piazza Leonardo da Vinci, Milan, Italy*
[b] *Department of Civil and Mechanical Engineering, Università degli Studi di Cassino e del Lazio Meridionale, Cassino, Italy*
[c] *School of Sustainability, Civil and Environmental Engineering, University of Surrey, Guildford, United Kingdom*

Abstract

A mechanistic model is presented for the strength prediction of squared columns made of masonry with a periodic arrangement and strengthened with a fibre-polymer composite jacketing. The formulation is based on an incremental plasticity theory that relies on equilibrium, compatibility, and kinematic equations. The strength domain of brick units and mortar joints is bounded by a multi-surface yield criterion: a Mohr-Coulomb strength domain with a linear cap in compression and a Rankine cut-off in tension. An elasto-plastic response with limited ductility is assumed for both masonry components. Differently, the FRP response is assumed elastic with a brittle failure governed by a limited tensile strain. Phenomenological-based assumptions are undertaken and justified. Details are also provided for the computational implementation of the procedure. The model accuracy is validated against experimental data on masonry squared columns and compared with existing standard-based formulas. Results demonstrate it provides real-time and accurate compressive strength solutions for squared masonry columns with or without a fibre-polymer composite wrapping and yet requiring few input parameters for the masonry constituents and reinforcement.

Keywords: Masonry columns, Masonry compressive strength, Fibre-polymer composites, Numerical modelling, FRP jacketing, fast structural assessment

*Corresponding author
Email address: luiscarlos.martinsdasilva@polimi.it (Luis C.M. da Silva)

Nomenclature

α	Strain increment correcting factor
β	Ratio between the current applied vertical stress in respect to the uni-axial compressive strength of the mortar
β_1	Threshold for the ratio β
κ	Ratio between the maximum σ_1 and the minimal σ_3 principal stresses
ν_b	Poisson's ratio for units
ν_m	Poisson's ratio for mortar
ν_{inf}	Lower bound limit of the Poisson's ratio for mortar
ν_{sup}	Upper bound limit of the Poisson's ratio for mortar
Ω_m	Mortar joints domain in the representative volume element
Ω_m	Unit domain in the representative volumelement
$\dot{\lambda}_k$	Plastic multiplier rate
$\dot{\sigma}_v$	Vertical stress increment
$\dot{\boldsymbol{\varepsilon}}_k^{b,pl}$	Plastic strain rate vector for units in time increment k
$\dot{\boldsymbol{\varepsilon}}_k^{m,pl}$	Plastic strain rate vector for mortar in time increment k
$\dot{\boldsymbol{\varepsilon}}_i^{(\cdot),e}$	Strain elastic increment
$\dot{\varepsilon}^{FRP}$	Elastic strain rate (horizontal direction) of the fibre-polymer composite wrapping
$\dot{\varepsilon}_h^{b,pl}$	Horizontal plastic strain rate for units in time increment k
$\dot{\varepsilon}_h^{m,pl}$	Horizontal plastic strain rate for mortar in time increment k
$\dot{\varepsilon}_v^{b,pl}$	Vertical plastic strain rate for units in time increment k
$\dot{\varepsilon}_v^{m,pl}$	Vertical plastic strain rate for mortar in time increment k
ϕ_b	Friction angle for the units
ψ_m	Internal dilation angle of mortar
ρ_s	Ratio of longitudinal steel reinforcement in the column cross-section
σ_{3l}	Mortar horizontal stress defined by the intersection of the compression cap and Coulomb criteria
$\tilde{E}_b$	Equivalent Young's modulus of the unit and fibre-polymer composite wrapping
$\boldsymbol{\sigma}_{k-1}^m$	Stress state in the mortar for time increment (k-1)
$\boldsymbol{\varepsilon}_k^{b,e}$	Elastic strain increment for units and for the time increment k
$\boldsymbol{\varepsilon}_k^{m,e}$	Elastic strain increment for mortar and for the time increment k
$\mathbf{f}_k$	Vector that controls the rate of the applied vertical strain for the increment k
$\mathbf{S}$	Global matrix that gathers the coefficients for the compatibility, constitutive and equilibrium equations
$\mathbf{x}_k$	Column vector that stores the unknown rates for the increment k
$\varepsilon_{cm,ult}$	Ultimate strain for uni-axial compression of mortar
$\varepsilon_{FRP,max}$	Maximum allowable tensile strain of the fibre-polymer composite wrapping
ε_i^e	Elastic part of the strain
ε_i^{pl}	Plastic part of the strain

A_c	Total area of the masonry column cross-section
A_e	Effective confined area of the masonry column cross-section
B	Cross section dimension of a squared masonry column
B_{eff}	Effective cross-section dimension of the masonry column
E_b	Young's modulus for units
E_m	Young's modulus for mortar
f_m^{cap}	Cap in compression for mortar
f_m^s	Coulomb failure in shear for mortar
$f_b^{t-Rankine}$	Rankine (tension) failure for units
f_{cb}	Uni-axial compressive strength of units
f_{cM}	Uni-axial compressive strength of the masonry
f_{cm}	Uni-axial compressive strength of mortar
f_{hcm}	Hydrostatic (tri-axial) compressive strength of mortar
$f_{l,eff}$	Umiformly applied effective pressure of the confinement
f_l	Maximum lateral confinement pressure
$f_{t,FRP}$	Uni-axial tensile strength of the FRP laminate
f_{tb}	Uni-axial tensile strength of units
G_{fcm}	Uni-axial compressive fracture energy of mortar
G_{ftb}	Uni-axial tensile fracture energy of units
H	Height of a squared masonry column
K	Hardening parameter
k_s	Coefficient that represents the ratio between the effectively confined area and the total cross-section area
$N_{\phi_m}^{\alpha}$	Slope for the linear failure envelope of mortar cap in compression
N_{ϕ_b}	Slope for the linear failure envelope of units in shear
N_{ϕ_m}	Slope for the linear failure envelope of mortar in shear
t	Thickness of mortar joints
t_k	Time increment k
t_{FRP}	Thickness for the FRP wrapping
TOL_{σ}	User-defined stress tolerance that deviates the stress path from the compressive failure envelope
FRP	Fiber Reinforced Polymer

1. Introduction

Unreinforced masonry typically exhibits relatively low strength and a quasi-brittle response in tension. These features determined its employment in vertical load-bearing structural elements whose stability is governed by compressive stresses [1–3], such as columns, walls and arches. The compressive strength of masonry can be found in laboratory through the construction and testing of stacked masonry prisms as preconized in the European standard EN 1052-1 [4], or even with larger setups as found in the literature [5]. Nonetheless, an accurate analytical prediction of the compressive strength is still a challenge due to the stress mismatch between the constituents [6, 7], being the approaches currently available for masonry columns grouped as semi-empirical, analytical, or numerical based.

Semi-empirical laws, as the ones presented by Haseltine [8] and more recently by Sarhat and Sherwood [9], are used in masonry code provisions [10, 11] owing its rationale to conservative assumptions. In this regard, the pioneering work of Hilsdorf [6] led to important experimental contributions that nurtured the onset of novel formulations. Hilsdorf proposed that an applied uni-axial compression stress leads to a tri-axial stress state within a masonry column. This theory was later on improved by Khoo and Hendry [7] to overcome the limitation of assuming that units and mortar have a similar strain at failure. Following such studies, McNary and Abrams [12] reported a comprehensive testing program for the tri-axial characterization of units and mortar, and analytical approaches have been developed after to include the effect of both masonry components. More recently, it is worth mentioning the research carried out by Drougkas et al. [13], in which a mechanistic-based micro-model with good accuracy was proposed to predict the strength of compressed masonry elements. More sophisticated analyses have been also explored, such as those retrieved from continuum-based Finite element (FE) strategies [14–16] or, for instance, the unravel of novel techniques based on machine learning-based methods [17].

The behaviour of masonry under pure compression is well documented [18–23], but the assessment of columns strengthened with a wrapping or jacketing technique deserves more insight. A typical solution is the use of FRP (Fibre-Reinforced Polymer), which is a strengthening system constituted by fibres glued to the support by means of a fibre-polymeric matrix. One can mention, for instance, the use of polymers reinforced with glass (GFRP), carbon (CFRP) and aramidic (AFRP) fibers. Textile reinforced mortar (TRM) or fabric reinforced cementitious matrix (FRCM) are also relevant alternatives since the inorganic matrix enables a higher material compatibility with the masonry substrate. The reader is referred to [24] for an insight on the advantages and disadvantages of each strategy. On one hand, it is rather clear that a jacketing-based retrofitting allows to improve both strength and ductility of masonry columns [18–21, 24–32]. On the other hand, some authors [33] address the concern over the accuracy of the existing analytical strategies when assessing the capacity of retrofitted columns.

In this context, several analytical models have been proposed to predict the behaviour of FRP and FRCM confined masonry columns [24, 34–37]. Despite such efforts, and as highlighted in [24, 38, 39], further investigations are required since some models were adapted from existing ones conceived for confined concrete columns [39]. Its accuracy is then dependent on ad-hoc calibrations over specific phenomenological-based parameters or constitutive laws aiming at representing different masonry types and jacketing natures [18–20, 24, 27, 40]. The Italian standard [35], alike with other existing formulas [19, 20, 40], includes provisions that are practical and simple to use, but for which it is required the knowledge of the un-confined (un-strengthened) compressive strength of the masonry material.

In overview, three research opportunities are identified from the literature. First, the opportunity to formulate a model that stems directly from hypotheses related with the mechanical behaviour of the masonry components, thence by-passing the use of concrete-related expressions as reported in [39]. Second, the opportunity to establish a predictive model for estimating the compressive strength of fiber-polymer composites in confined elements without relying on the unconfined (un-strengthened) compressive strength of the masonry. Third, the opportunity to present a reliable model for unconfined and fiber composite confined masonry squared columns, valid for different masonry and strengthening properties and for different dimensions for brick units and mortar joints.

In this context, this study presents a numerical model to estimate the compressive strength of un-confined and confined masonry columns with a fibre-polymer composite wrapping. We are bounded by the following hypotheses: (i) the masonry has a periodic arrangement, (ii) the masonry column has a squared transversal section; and (iii) the retrofitting is based on a fibre-polymer composite wrapping technique. Following the aforementioned research opportunities identified from the literature [33, 39], the proposed model must be accurate and computational efficient. A Finite Element (FE) micro-modelling approach is thus precluded [41]. Instead, a mechanistic-based model is pursued and able to reproduce: (i) the elasto-plastic behaviour of units and mortar joints; (ii) the non-linear elastic response of mortar due to the change of its Poisson's ratio according to the tri-axial compression state; (iii) failure of the units and mortar joints according to a multi-surface failure domain with either an associated and non-associated plastic flow rule; and (iv) an elastic response with a brittle failure for the composite wrap. Furthermore, the strategy includes the mechanical properties of mortar and units as input (instead of the compressive strength of the unreinforced masonry), as it is more convenient because it is easier and faster to perform mechanical characterization tests on the masonry components. Aiming at reducing the number of input parameters, some phenomenological-based assumptions are introduced, but generally sustained by appropriate literature evidence. At last, attention is given to validate the model using data from several experimental campaigns that correspond to different masonry types, different columns geometries, different number of layers and nature of the fibre-polymer composite wrapping.

2. Mechanics of periodic masonry in compression

The mechanics of periodic masonry in compression is reviewed in this section for both the un-strengthened and strengthened cases. Important remarks found via laboratory tests are summarized since they are paramount to understand and support adopted assumptions in the development of the proposed strategy.

2.1. Un-strengthened masonry columns

Hilsdorf's research shed light on the fundamental mechanism underlying masonry compression failure, revealing that it emerges from the intricate interplay between the brick units and mortar bed joints. Experimental data corroborate that brick units generally have a greater compressive strength and a lower Poisson's ratio than mortar joints. Under compression, the bed mortar joints tend to expand laterally, but the less deformable units restrict such lateral expansion. This gives rise to a state of pure tri-axial compression in the mortar joints and a state of compression-tension-tension in brick units, as depicted in Fig. 1.

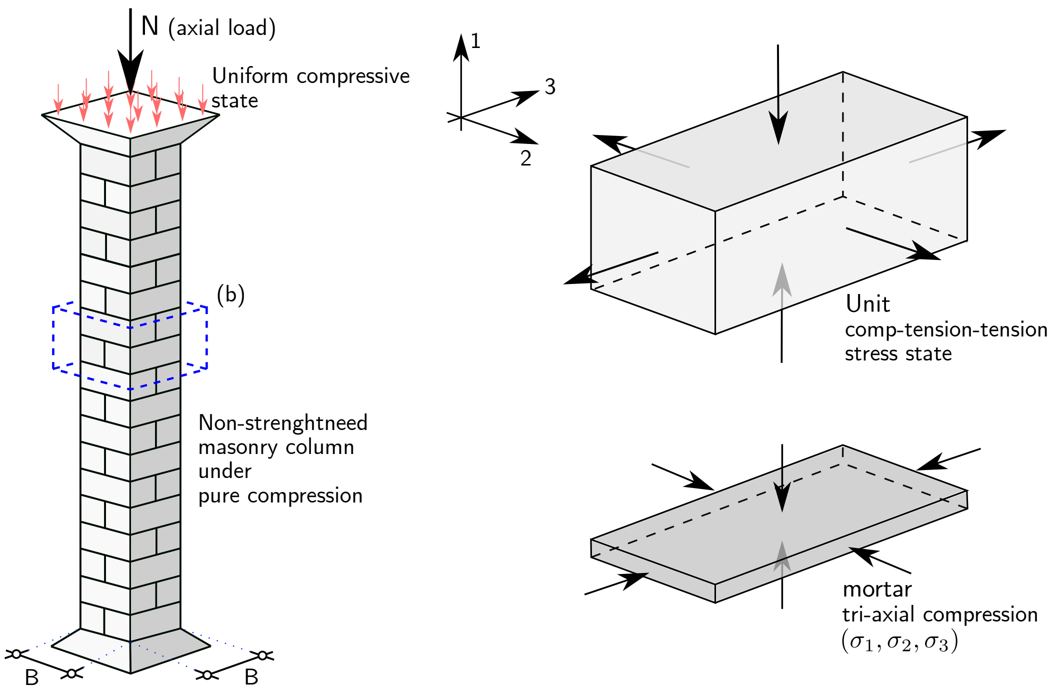

(a) masonry column

(b) stress-state in the masonry components

Figure 1: Un-strengthened squared masonry column.

Predicting the compressive strength of masonry is challenging due to the stress states mismatch and the varying material and geometric properties of its constituents. However, the non-linear response of mortar can not be overlooked. Studies by Khoo et al. [7] and McNary et al. [12] have focused on understanding the response of mortar under tri-axial compression. Khoo et al. [7] reported that the compressive stress-strain curve remains relatively linear until 40%-60% of the ultimate strength, beyond which major microcracking occurs thence leading to increased strains that correspond to the flattening of the capacity curve. McNary et al. [12] demonstrated that mortar dilatancy leads to increased tensile lateral stresses and a reduction in vertical compressive stress, which modifies the failure mode of masonry. Experimental data also supports the notion that confinement effects are more pronounced in masonries with more deformable mortars, in which the cement content seems paramount.

Recent studies on mortars under tri-axial compression have addressed two important observations: (i) the type and composition of mortar influences the failure mode, and (ii) the elastic mechanical properties of mortar are influenced by the confining pressure. In this regard, it is generally found that a brittle behaviour is observed for stronger mixes ('strong mortars') associated with an increase in compressive strength due to confinement [13, 42, 43]. In contrast, a relatively higher ductility is found for weaker mixes ('weak mortars'). In the presence of low confinement levels, a failure envelope governed by shear mechanisms is identified and a Mohr-Coulomb envelope fits well. For a greater lateral confinement and compressive stresses, the failure is governed by crushing. The so-called 'discontinuity point' that bounds the two observed failures ranges in the vicinity of $\kappa = \frac{\sigma_3}{\sigma_1} = 0.25$ [42, 44]. From experimental data, a failure envelope in tri-axial stress state that resembles a Mohr-Coulomb envelope with a linear slope has been found, which is in line with the hypothesis from *Khoo's et al.* [7], i.e. that the mechanics of mortar after the discontinuity point is primarily one of inter-particle friction.

Regarding the effect of the confining pressure, it appears to have an influence on the magnitude and variation of the isotropic elastic constants, i.e. Young's modulus and Poisson's ratio [13, 43, 45, 46]. Although studies on the variation of the Young's modulus are scarce, the variation of the Poisson's ratio is well evidenced. Studies report that the variation of the Poisson's ratio is less pronounced in weak mortars and is generally attributed to microscopic causes due to porosity and the existence of voids [12, 43, 47]. The transition zone between grain and cement-paste is reported to be the most porous component of the media. Such porosity is dependent on the composition, water/cement ratio, maximum diameter, and grain size distribution of the sand [48]. Therefore, some researchers observed that the Poisson's ratio decreases for low confinement stresses [7, 47, 49] and, after a threshold, tends to increase significantly until failure, reaching values of 0.8-0.9 [43]. Thence, a linear approach [50] is unsuitable to predict the mechanical response of mortar in a tri-axial compression state since a constant Poisson's ratio does not represent the volume change of the mortar that generally occurs when it reaches the uni-axial compressive strength level [51]. Although limited numerical models have been developed to account for this change, it is still considered critical. This variation may be included using the model proposed by Ottosen [52] for concrete, or through other proposals that are better suited for mortars [46, 51].

2.2. Fibre-Polymer composite wrapping of masonry columns

The improvement on both strength and ductility of brick masonry columns through a fibre-polymer composite wrapping retrofit is well evidenced in the literature. The efficiency of the strengthening is yet dependent on several variables, such as the type of fibers, the number of layers, the wrapping strategy (continuous or discontinuous layers), the overlapping length, and the cross-section dimensions and corner radius [18–21, 24, 27–31, 53–55].

Two remarks are generally established in the existing strategies to predict the ultimate capacity of non-circular masonry columns confined with a fibre-polymeric based wrapping: (i) the assumption of constant confining pressure should be disregarded in the case of FRP-wrapping [33, 39]; and (2) the consideration of an effective pressure of the confinement $f_{l,eff}$ that is uniformly applied, which is dependent on geometric features of the column and mechanical properties of the masonry constituents. Proposals are available in various studies [56, 57], but it appears consensual to calculate $f_{l,eff}$ according to:

$$f_{l,eff} = k_s f_l \tag{1}$$

in which k_s is a coefficient that represents the ratio between the effectively confined area and the total cross section area; and f_l is the maximum possible lateral confining pressure exerted by the confinement. The expression to compute k_s is well diffused and consensual and the main difficulty arises when finding the value for the lateral confinement pressure f_l as demonstrated in [27, 33, 39, 40, 57].

The constitutive relationship for the polymeric-base can be established as a linear elastic in tension [29, 56], in which a brittle failure appears to be consistent with experimental evidence [33, 39]. Experiments highlight that fibre-polymer composites tend to fail for stress levels far below the ultimate tensile strength $f_{t,FRP}$. The most common failure modes are addressed as follows [38, 39]: (1) rupture of the composite laminates due to the dilation of the masonry; (2) detachment of the composite laminates due to reduced overlapping length or anchoring of the wrapping; (3) local buckling of the wrapped laminates and local crushing of the masonry unit or mortar; and (4) the dilation of the masonry under compression and the development of hoop tensile stresses in the composite laminates that lead to the so-called 'tearing' or 'knife' effect in the corners [58, 59].

3. Formulation of the numerical model

A numerical model for the compressive strength prediction of squared masonry columns is presented in this section. The formulation, together with the main theoretical assumptions, are addressed for both un-strengthened and strengthened cases. A framework based on the incremental theory of plasticity with an appropriate yield function, which includes both tension and compression responses for the masonry components, is adopted. First, it is noteworthy to recall that the current experimental literature on masonry columns is significant and tends to address the capacity of squared, rectangular, octahedral, and circular columns with a periodic arrangement of brick/block units. The different geographic sources of such studies, as extensively reported in [39], underline the importance of these elements in existing masonry structures of different periods. In specific to squared cross-sections, its use can be identified in many existing masonry buildings and some examples can be found in Italy in cloisters, in internal or external colonnades of buildings, among others, as presented in [60–62] for buildings that range from the 15th to the 19th centuries.

3.1. Un-strengthened squared masonry column

An elasto-plastic representative volume element (RVE) that occupies a domain $\Omega \in \mathbb{R}^3$ at initial time t_0 is considered for the modelling of a periodic type of masonry that represents a squared column under uni-axial compression. From *Hilsdorf's* theory [63], the stress state in the masonry components is characterized by tri-axial compression for mortar and compression-tension-tension for brick units (Fig. 1). The formulation is thus provided in terms of principal strain and stress quantities. In specific and using *Voigt's* notation, the generalized stress and strain components are given as $\boldsymbol{\sigma} = [\sigma_1,\ \sigma_2,\ \sigma_3]$ and $\boldsymbol{\varepsilon} = [\varepsilon_1,\ \varepsilon_2,\ \varepsilon_3]$, respectively. Moreover, this stress state assumption asserts that brick units must exhibit lower deformability compared to mortar joints. The applicability of the model is then restricted to cases where the Poisson's coefficient of mortar exceeds that of the brick units, i.e. $\nu_m > \nu_b$.

The RVE of the unit cell is modelled through a stack-bond approach (Fig. 2), thence neglecting the effect of potential head joints [64]. Two remarks are noteworthy. First, this assumption underpins the practical nature of the strategy, in which the modelling time required by a direct numerical simulation using a Finite-Element (FE) model [16] or Discrete Element model (DEM) [**?**] is avoided. Geometric parameters serve directly as input for the formulation. Secondly, the adoption of a stack-bond for the RVE, together with the particular study of squared masonry columns, allows to theoretically state that $\sigma_2 = \sigma_3$. Note, however, that even for non-squared columns or walls, the assumption of alike transverse stresses is presented in the literature [65]. Therefore, and for the sake of readiness, it is indicated hereafter that $\sigma_1 = \sigma_v$,$\sigma_2 = \sigma_3 = \sigma_h$, in which the subscript v and h refers to vertical and horizontal directions, respectively.

An incremental approach is presented, in which the stress state $\boldsymbol{\sigma}$ is evaluated for both mortar (Ω_m) and brick (Ω_b) constituents at each time increment t_k. The time variable $t \in [0, t_{max}]$ controls the prescribed increment of vertical strain $\Delta\varepsilon_v$ applied to the boundary Γ_D, which is established and assumed as known at the beginning of each k increment. Although $\boldsymbol{\varepsilon} := \boldsymbol{\varepsilon}(t)$ and $\boldsymbol{\sigma} := \boldsymbol{\sigma}(t)$, these are considered to be equal at any point $\mathbf{P} \in \Omega_m$ and $\mathbf{P} \in \Omega_b$ for a given time increment t_k.

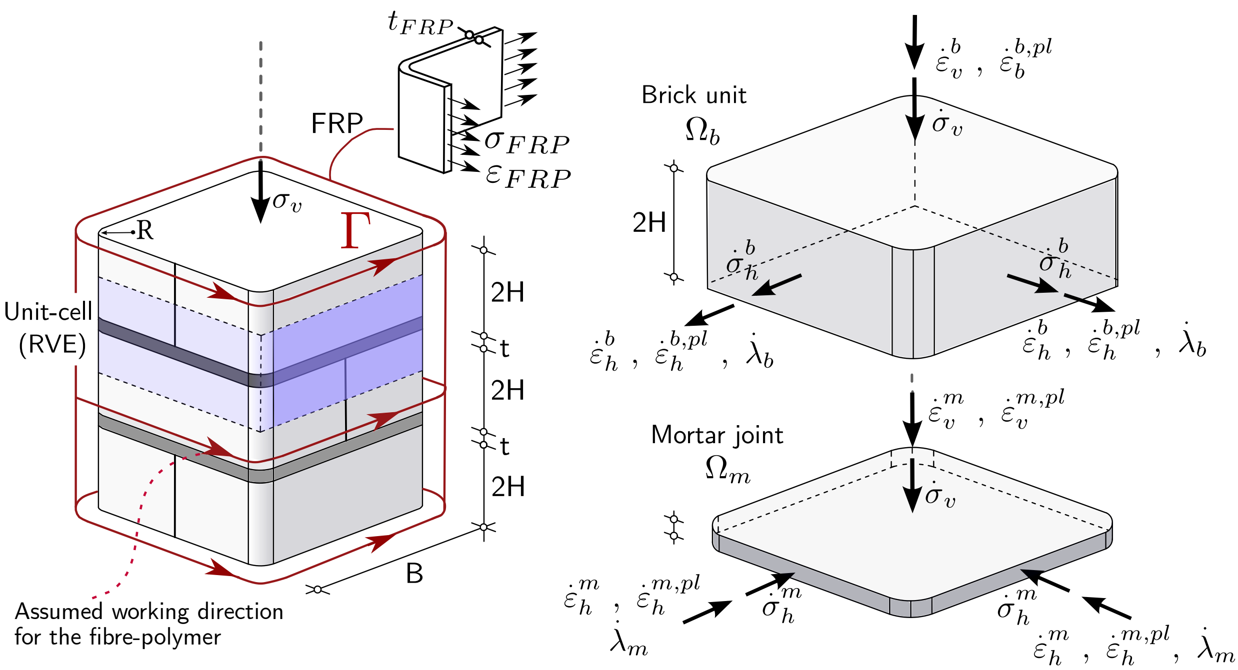

Figure 2: Representative Volume Element (RVE) and variables of the system.

The strain vector is calculated assuming an additive decomposition of the elastic ε_i^e and plastic ε_i^{pl} parts of strain, such that:

$$\boldsymbol{\varepsilon} = \boldsymbol{\varepsilon}^e + \boldsymbol{\varepsilon}^{pl} \tag{2}$$

Accordingly, the strain variation (expressed in rate form) for each k^{th} increment is found as:

$$\dot{\boldsymbol{\varepsilon}}_i^{(\cdot)} = \dot{\boldsymbol{\varepsilon}}_i^{(\cdot),e} + \dot{\boldsymbol{\varepsilon}}_i^{(\cdot),pl} \quad , \ (\cdot) = m, b \ \text{ and } \ i = v, h \tag{3}$$

in which the elastic increment $\dot{\boldsymbol{\varepsilon}}_i^{(\cdot),e}$ is determined according to a constitutive relationship based on the *Hooke's* law. In specific, the time-independent relation for brick units is given in Eq. (4a) and written according to the corresponding Young's modulus E_b and Poisson's ratio ν_b. For mortar, the relation is given in Eq. (4b). The Young's modulus E_m is kept constant, but the Poisson's ratio can be defined by a time-dependent law $\nu_m(\boldsymbol{\sigma}^m)$ as it is described in section 3.3. The inclusion of such internal variable is paramount to describe the non-linear elastic response of some mortars for higher confinement stresses; a critical behaviour that was highlighted in section 2.

$$\boldsymbol{\varepsilon}_k^{b,e} = [\dot{\varepsilon}_h^{b,e} \ , \ \dot{\varepsilon}_v^{b,e}]^T = \frac{1}{E_b}\begin{bmatrix} 1-\nu_b & -\nu_b \\ -2\nu_b & 1 \end{bmatrix}\begin{bmatrix} \dot{\sigma}_h^b \\ \dot{\sigma}_v^b \end{bmatrix} \tag{4a}$$

$$\boldsymbol{\varepsilon}_k^{m,e} = [\dot{\varepsilon}_h^{m,e} \ , \ \dot{\varepsilon}_v^{m,e}]^T = \frac{1}{E_m}\begin{bmatrix} 1-\nu_m(\boldsymbol{\sigma}_{k-1}^m) & -\nu_m(\boldsymbol{\sigma}_{k-1}^m) \\ -2\nu_m(\boldsymbol{\sigma}_{k-1}^m) & 1 \end{bmatrix}\begin{bmatrix} \dot{\sigma}_h^m \\ \dot{\sigma}_v^m \end{bmatrix} \tag{4b}$$

The total strain for both masonry components is found by respecting the interface compatibility condition according to *Hilsdorf's* theory [6]. Strain equality is enforced in the horizontal direction in Eq. (5) and vertical direction in Eq. (6).

$$\dot{\varepsilon}_h^{b,e} + \dot{\varepsilon}_h^{b,pl} = \dot{\varepsilon}_h^{m,e} + \dot{\varepsilon}_h^{m,pl} \tag{5}$$

$$\dot{\varepsilon}_v(2H + t) = 2H(\dot{\varepsilon}_v^{b,e} + \dot{\varepsilon}_v^{b,pl}) + t(\dot{\varepsilon}_v^{m,e} + \dot{\varepsilon}_v^{m,pl}) \tag{6}$$

The horizontal equilibrium is verified globally given the system components as follows:

$$2HB\dot{\sigma}^b_{xx} + tB\dot{\sigma}^m_{xx} = 0 \tag{7}$$

in which B and H are, respectively, the cross-section dimension and the half-height of units. From the vertical stress equilibrium, one can assume that $\dot{\sigma}_v = \dot{\sigma}^b_v = \dot{\sigma}^m_v$. The admissible set of principal stresses for both mortar and units is bounded by a closed and convex domain f, in which $f : \mathbb{R}^n \mapsto \tilde{f} \in \mathbb{R}$. A multi-surface approach is adopted as depicted in Fig. 3 and provided in the $\sigma_1 - \sigma_3$ space under the condition that $\sigma_1 \leq \sigma_2 = \sigma_3$. For the un-strengthened case, the shape and size of f remains fixed during the loading history.

Mortar stress state is restricted to the third quadrant of the $\sigma_1 - \sigma_3$ space and is governed by a Coulomb failure in shear (f^s_m) and a cap in compression (f^{cap}_m):

$$f^s_m(\boldsymbol{\sigma}^m) = -\sigma_1 + \sigma_3 N_{\phi_m} - f_{cm} \tag{8a}$$

$$f^{cap}_m(\boldsymbol{\sigma}^m) = -\sigma_1 + \sigma_3 N^\alpha_{\phi_m} - (1 - N^\alpha_{\phi_m}) f_{hcm} \tag{8b}$$

such that f_{cm} is the uni-axial compressive strength of mortar; f_{hcm} the value for which the hydrostatic (tri-axial) compressive strength of mortar is found; and N_{ϕ_m} and $N^\alpha_{\phi_m}$ the slopes corresponding to the linear envelopes and given by:

$$N_{\phi_m} = \frac{1 + \sin(\phi_m)}{1 - \sin(\phi_m)} \quad , \quad N^\alpha_{\phi_m} = \frac{3f_{cm} + \frac{4f_{cm}}{N_{\phi_m}-4}}{3f_{cm} + \frac{f_{cm}}{N_{\phi_m}-4}} \tag{9}$$

in which $N^\alpha_{\phi_m} \geq 0$. Here, two remarks are important to address: (i) experimental evidence supports the assumption that $f_{hcm} = 3f_{cm}$ (see Appendix C), which appears representative for different types of mortar, as hydrated lime mortar, hydraulic lime mortar, and hybrid mortar [42]; (ii) a linear cap has been adopted, even though experimental evidence demonstrates the good fitness of a parabolic or ellipsoidal curve [42, 43]; and (iii) the linear cap slope is assumed to be null or positive and found through the intersection between the Mohr-Coulomb shear criterion with the $\kappa = 0.25$ stress curve. Experimental evidence supports such assumption since for stress values in the vicinity of $\kappa = 0.25$, the observed failure passes from a fragile one (shear) to a ductile (crushing) one [42].

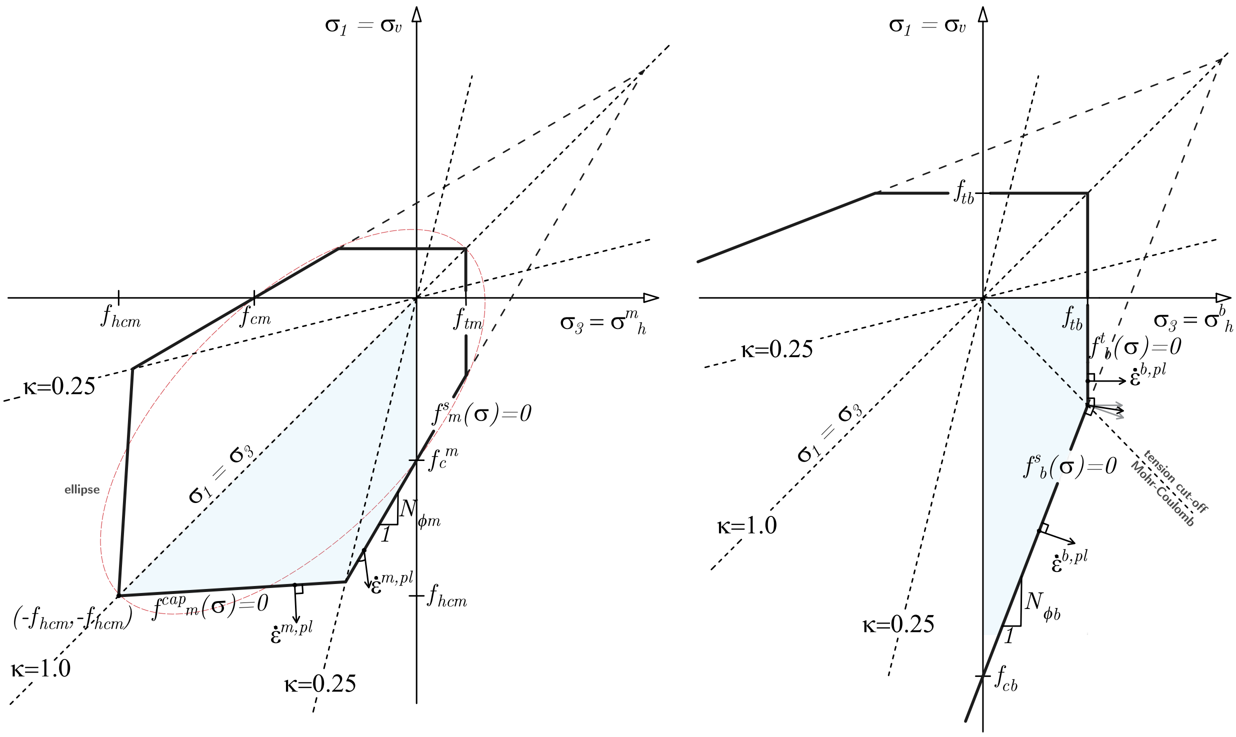

(a) mortar joints (b) brick units

Figure 3: Multi-surface failure criteria adopted for masonry components ($\kappa = \frac{\sigma_3}{\sigma_1}$).

For brick units, a Mohr-Coulomb failure (f_b^s) with a tension cut-off (f_b^t) is considered:

$$f_b^s(\boldsymbol{\sigma}^b) = -\sigma_1 + \sigma_3 N_{\phi_b} - f_{cb} \tag{10a}$$

$$f_b^t(\boldsymbol{\sigma}^b) = \sigma_3 - f_{tb} \tag{10b}$$

in which f_{cb} and f_{tb} are, respectively, the uni-axial compressive and tensile strength of units. The shear failure slope in Eq. (11) for the units is function of the associated internal friction angle ϕ_b .

$$N_{\phi_b} = \frac{1 + \sin(\phi_b)}{1 - \sin(\phi_b)} \tag{11}$$

Mortar and brick units remain in an elastic state when $f_{(\cdot)}(\boldsymbol{\sigma}) < 0$. Failure or the onset of plasticity – depending on the adopted constitutive responses given in section 3.3 – requires that one of the criteria surfaces is active, such that $f_{(\cdot)}(\boldsymbol{\sigma}) = 0$. For mortar, the plastic relations are described through a flow-rule associated in compression (f_m^{cap}) with general form of Eq. (12) but non-associated with the failure surface in shear (f_m^s) as presented in Eq. (13). For brick units, the plastic flow-rule is associated with all the failure functions and thus follows the form given in Eq. (12).

$$\dot{\boldsymbol{\varepsilon}}_k^{(\cdot),pl} = \dot{\lambda}_k^{(\cdot)} \frac{\partial f}{\partial \sigma_i} \quad , \quad i = 1,3 \quad and \quad (\cdot) = b, m \tag{12}$$

$$\dot{\boldsymbol{\varepsilon}}_k^{m,pl} = \dot{\lambda}_k^{m} \frac{\partial g}{\partial \sigma_i} \quad , \quad i = 1,3 \tag{13}$$

in which $\dot{\boldsymbol{\varepsilon}}_k^{b,pl} = [\dot{\varepsilon}_h^{b,pl} \ , \ \dot{\varepsilon}_v^{b,pl}]^T$ and $\dot{\boldsymbol{\varepsilon}}_k^{m,pl} = [\dot{\varepsilon}_h^{m,pl} \ , \ \dot{\varepsilon}_v^{m,pl}]^T$ are, respectively, the plastic strain rate vector for brick and mortar for the k^{th} increment; $\dot{\lambda}_k$ the plastic multiplier rate at each increment k and respects the Kuhn-Tucker complementary conditions of Eq. (14):

$$f(\boldsymbol{\sigma}^{(\cdot)}) \leq 0 \qquad \dot{\lambda}_k \geq 0 \qquad \dot{\lambda}_k f(\boldsymbol{\sigma}^{(\cdot)}) = 0 \tag{14}$$

meaning that an elastic state is characterized by $\dot{\lambda}_k = 0$ and $f_{(\cdot)}(\boldsymbol{\sigma}) < 0$ and a plastic state is initiated when $\dot{\lambda}_k > 0$ and $f_{(\cdot)}(\boldsymbol{\sigma}) = 0$. The function g is defined in terms of the internal dilation angle of mortar ψ_m, i.e.:

$$g_m^s(\boldsymbol{\sigma}^m) = -\sigma_1 + \sigma_3 \frac{1 + \sin(\psi_m)}{1 - \sin(\psi_m)} - f_{cm} \tag{15}$$

In the domain singularities, an additive operation between the normals of both surfaces is assumed as presented in Fig. 3: (1) intersection between $f_m^s < 0$ and $f_m^{cap} < 0$ and (2) intersection between $f_b^s < 0$ and $f_b^{t-Rankine} < 0$.

At last, it is remarked that the Mohr-Coulomb criteria is written directly in terms of tensile and compressive strengths. This is convenient since most experimental data provides values from the compressive and tensile material characterization tests. This allows to directly fulfil the input of the numerical model, thence to bypass the limitation of the general formulation that adopts the cohesion parameter.

3.2. Strengthened masonry with a fibre-polymer composite

The contribution of the fibre-polymer composite is included by adding the corresponding strain and stress terms in the compatibility and equilibrium equations of the system. In specific, from strain compatibility between the FRP wrapping and the brick unit:

$$\dot{\varepsilon}_h^{b,e} + \dot{\varepsilon}_h^{b,pl} = \dot{\varepsilon}^{FRP} \tag{16}$$

in which $\dot{\varepsilon}^{FRP}$ is the elastic strain rate (horizontal direction) of the fibre-polymer wrap. Accordingly, the horizontal equilibrium is re-written as:

$$2HB\dot{\sigma}_{xx}^{b} + tB\dot{\sigma}_{xx}^{m} + t_{FRP}(2H + t)\dot{\sigma}_{FRP} = 0 \tag{17}$$

in which $\dot{\sigma}_{FRP}$ is the axial (membrane) stress rate in the wrapping system. The existence of the strengthening affects both the horizontal stiffness of the system and the lateral strength, i.e. the so-called confinement effect. The first is included by providing an equivalent stiffness for the unit-wrapping system and readjusting the elastic constitutive relationship for the units:

$$\boldsymbol{\varepsilon}_k^{b,e} = [\dot{\varepsilon}_h^{b,e}\ ,\ \dot{\varepsilon}_v^{b,e}]^T = \begin{bmatrix} \frac{1-\nu_b}{\tilde{E}_b} & -\frac{\nu_b}{\tilde{E}_b} \\ \frac{-2\nu_b}{E_b} & \frac{1}{E_b} \end{bmatrix} \begin{bmatrix} \dot{\sigma}_h^b - 2\dot{\sigma}_{FRP}(\frac{t_{FRP}}{B-2R}) \\ \dot{\sigma}_v^b \end{bmatrix} \tag{18}$$

such that $\tilde{E}_b$ is found according to the rule of mixtures [66] ('Voigt' type [67]) and given as:

$$\tilde{E}_b = \frac{2t_{FRP}E_{FRP}^2 + BE_b^2}{2t_{FRP}E_{FRP} + BE_b} \tag{19}$$

in which E_{FRP} is the Young's modulus of the fibre-polymer in the direction parallel to mortar bed joints as given in Fig. 2. Concerning the increase in the strength of the system due to the lateral confinement provided by the polymeric-wrapping, this is included by offering an expansion on the initial yield domain of the unit through an isotropic hardening approach. Differently from the un-strengthened case, the shape and size of the yield locus is affected by the loading history through a hardening parameter. In specific, the hardening law is dependent on the effectively confined area of the column cross-section, thence somehow aligned with classical approaches that make use of this parameter. In this regard, k_s is function of the ratio of effectively confined area A_e to the cross sectional area, A_c. The shape factor can be expressed as [68]:

$$k_s = \frac{A_e}{A_c} = 1 - \frac{2B_{eff}^2}{3(B^2 - \frac{\pi R^2}{3})(1 - \rho_s)} \tag{20}$$

in which R is the radius of the corner, B_{eff} is the effective cross-section dimension calculated as $B_{eff} = B - 2R$, and ρ_s

is the ratio of longitudinal steel reinforcement in the cross-section (herein $\rho_s = 0$). The yield surfaces for brick units is, in the presence of wrapping, defined as:

$$f_b^s(\boldsymbol{\sigma}^b, K_k) = -\sigma_1 + N_{\phi_b}(\sigma_3 - k_s K_k) - f_{cb} - k_s K_k \tag{21a}$$

$$f_b^t(\boldsymbol{\sigma}^b, K_k) = \sigma_3 - f_{tb} - k_s K_k \tag{21b}$$

in which K_k is the hardening parameter in the k^{th} increment and depends on the effective lateral confinement. Here, the Kuhn-Tucker complementary conditions expressed in Eq. (14) must also hold. Since the formulation is provided in rate form, the updated yield criteria is directly found at the end of the time increment:

$$K_k = \frac{2(\varepsilon_{FRP} E_{FRP}) t_{FRP} (2H + t)}{HB\nu_b} \tag{22}$$

in which ε_{FRP} is the total strain in the FRP for the k^{th} instant. It is considered that the FRP fails when the dilation effect of the masonry leads to $\varepsilon_{FRP} > \varepsilon_{FRP,max}$. The most common failure modes observed for the FRP are addressed in section 2.2. The proposed formulation is able to reproduce the rupture of the composite laminates due to the dilation of the masonry. However, the formulation is unable to explain the 'per causa' of detachment of the composite laminates due to reduced overlapping length, the possibility of local buckling of the wrapped laminates and the so-called 'tearing' or 'knife' effect in the corners [58, 59]. Instead, these are considered by following the Italian normative recommendations [35], such that $\varepsilon_{FRP,max} = 0.004$ (ignoring any safety factor). Better results are found for the case of CFRP wrapping when it is considered that $\varepsilon_{FRP,max} = 0.8\frac{f_{t,FRP}}{\bar{E}_b}$ such that $\varepsilon_{FRP,max} \geq 0.004$ ($f_{t,FRP}$ is the uni-axial tensile strength of the fibre-polymer base and it is found experimentally). Such observations may be associated with the 'knife' effect that is the critical failure mode when carbon fibres are used.

3.3. Adopted constitutive laws and Poisson's ratio of mortar

The adopted constitutive relationships for the system components try to include the experimental evidence reported in section 2. The fibre-polymer composite is assumed to follow a linear elastic and brittle response. Again, the maximum allowable tensile strain ε_{FRP} is limited to $\varepsilon_{FRP,max} \geq 0.004$ or, in the particular case of a CFRP for a more accurate prediction, limited to $\varepsilon_{FRP,max} = 0.8\frac{f_{t,FRP}}{\bar{E}_b}$ such that $\varepsilon_{FRP,max} \geq 0.004$. Brick units are considered to follow an elastic-perfectly plastic response with limited ductility, being the fracture energy of the post-peak plateau computed according to literature recommendation [69] as:

$$G_{ftb} = 0.07\ln(1 + 0.17 f_{cb}) \tag{23}$$

For mortar joints, the response is slightly more complex. An elasto-perfectly plastic law with limited ductility is also assumed. Nonetheless, the ultimate strain of the mortar in confinement conditions ε^u_{cm} is written in terms of the ultimate strain for uni-axial compression $\varepsilon_{cm,ult}$, such that $\varepsilon_{cm,ult} = \frac{f_{cm}}{E_m} + \frac{G_{fcm}}{Bf_{cm}}$, in which G_{fcm} is the compressive fracture energy of the mortar. This parameter can be computed according to Eq. (24) [70] if the experimental data is unavailable.

$$G_{fcm} = \frac{32 f_{cm}}{10 + f_{cm}} \tag{24}$$

And, in order to include an increase of the brittleness observed at higher confinement levels, the ultimate strain of the mortar in confinement conditions is given by:

$$\varepsilon^u_{cm} = \varepsilon_{cm,ult}\frac{\sigma_3 - \sigma_{3l}}{\sigma_{3l}}\langle\sigma_3 - \sigma_{3l}\rangle^0 \quad , \quad \sigma_{3l} = \frac{f_{cm}(3N^\alpha_{\phi_m} - 2)}{N_m - N^\alpha_{\phi_m}} \tag{25}$$

in which $\langle\cdot\rangle$ are Macaulay brackets and σ_{3l} is the horizontal stress defined by the intersection of the compression cap and Coulomb criteria as depicted in Fig. 3. The formulation allows to respect the observed experimental evidence reported in section 2, i.e. a brittle response when the failure of mortar is governed by the compression cap ($\sigma_3 > 0.25\sigma_1$) and, an increased brittleness under (through a linear relation) higher confinement levels in the case that mortar yielding is governed by the Mohr-Coulomb criteria ($\sigma_3 < 0.25\sigma_1$). Such approach is aligned with a strategy that keeps the $\varepsilon_{cm,ult}$ value fixed independently of the stress state, as seen in [46].

To what concerns the elastic non-linear response that mortar features before failure, it is herein described by the variation of the Poisson's ratio according to the stress level, as anticipated in Eq. (4b). Note that, although the initial Young's modulus of mortar appear to vary as well, the initial value is kept constant for the sake of simplicity and to maintain a reduced number of input variables. The use of a constant Poisson's ratio for mortar blurs the accuracy of numerical models when predicting the compressive strength of masonry with strong mortars. In this regard, the formulas proposed by Ottosen [52] and by Mohamad [47] are here adapted to reproduce: (i) the initial decrease in the Poisson's ratio ν_m, (2) the significant increase of ν_m after the uni-axial compressive strength value, and (3) the rapid increase of ν_m near failure, in which very high values can be reached, i.e. ν_{sup} of $\approx 0.8 - 0.9$.

$$\nu_m^k(\beta) = \begin{cases} \nu_{inf} & if \quad \beta \leq \beta_1 \\ \nu_m - (\nu_m - \nu_{inf})\sqrt{(1 - \frac{\beta-\beta_1}{1-\beta_1}} & if \quad \beta_1 \leq \beta \leq 1.0 \\ \nu_m & if \quad \beta \geq 1.0 \ \wedge \ f_m^{cap}(\boldsymbol{\sigma}_{k-1}^m) < TOL_\sigma \\ \nu_{sup} & if \quad \beta \geq 1.0 \ \wedge \ f_m^{cap}(\boldsymbol{\sigma}_{k-1}^m) \geq TOL_\sigma \end{cases} \tag{26}$$

in which β is the ratio of the current applied vertical stress in respect to the uni-axial compressive strength of the mortar; β_1 is the threshold defined as $\beta_1 = 0.8 f_{cm}$ [46, 47, 52]; $f_m^{cap}(\boldsymbol{\sigma}_{k-1}^m)$ is the function value associated with the mortar compression cap and TOL_σ a user-defined tolerance. This tolerance defines a distance to the failure envelope for which the mortar stress path deviates and it is herein assumed to be $0.2 f_{cm}$. At last, one addresses that in the case that a weak mortar is considered, then the Poisson's ratio is kept constant and given as ν_m.

3.4. Elastic predictor and returning map

For a time step increment k for which the state of the mechanical constituent of the system is still elastic, then the increment of vertical strain is provided under the condition that the corresponding plastic-flow is inexistent ($\dot{\lambda}_k = 0$). The compatibility and equilibrium equations are solved by assuming a trial vertical strain $\dot{\varepsilon}_v^{e,tr}$ that allows to find the trial stress state $\boldsymbol{\sigma}_{k+1}^{tr}$ of the system. In the case $f(\boldsymbol{\sigma}_{k+1}^{tr}, K_{k+1}) \leq 0$, the Kuhn-Tucker conditions of Eq. (14) are satisfied and the computed stress represents the actual stress of the system. Otherwise, the trial stress lies outside the yield loci when $f(\boldsymbol{\sigma}_{k+1}^{tr}, K_{k+1}) > 0$ and a plastic corrector step is required.

Studies demonstrate that a closed-formed solution based on a radial-map returning can be found for specific problems [71, 72]. More general frameworks based on a closest-point projection are also extensively studied [73, 74] since it constitutes a variational form through the distance minimization between the trial stress and the function that represents the set of admissible stress states. In this study, a straightforward and simple strategy is drawn owing to the particularities of the problem. The defined scheme allows to obtain an exact solution in a single step and thence avoiding the need of an iterative procedure. This is possible because a strain-driven formulation based on the increment of a single variable $\dot{\varepsilon}_v$ is assumed, and because the mechanical problem is formulated with a set of linear equations.

The method involves finding a return mapping factor that is computed considering the scalar values of the critical failure function of the time increment k and $k+1$. A relevant assumption is that the correction is processed following the same direction of the stress path defined between the stress state for those increments as given in Fig. 4. The corrected trial vertical strain for the k^{th} time increment must satisfy the condition $f(\boldsymbol{\sigma}_{k+1}, K_{k+1}) = 0$, in which $\boldsymbol{\sigma}_{k+1} = \boldsymbol{\sigma}_k + \dot{\boldsymbol{\sigma}}_{k+1}^{tr}$, and reads:

$$\dot{\varepsilon}_{v,k+1}^{e,corrected} = \alpha \dot{\varepsilon}_v^{e,tr} \ \Rightarrow \ \lambda_{k+1}^{(\cdot),corrected}, \ \dot{\boldsymbol{\sigma}}_{k+1}^{(\cdot),corrected} \tag{27}$$

in which α is the corrector factor and it is linearly dependent on the scalar value of the active failure surfaces, such that:

$$\alpha = \left| \frac{\tilde{f}_k}{\tilde{f}_{k+1} - \tilde{f}_k} \right| \tag{28}$$

and $\tilde{f}_k = f(\boldsymbol{\sigma}_k)$ and $\tilde{f}_{k+1} = f(\boldsymbol{\sigma}_{k+1})$. Here, by active surface it is referred the specific function that defines the composite yield domain with a positive value, i.e. among Eq. (8) and Eq. (10) for the un-strengthened case, and Eq. (8) and Eq. (21) for the strengthened case.

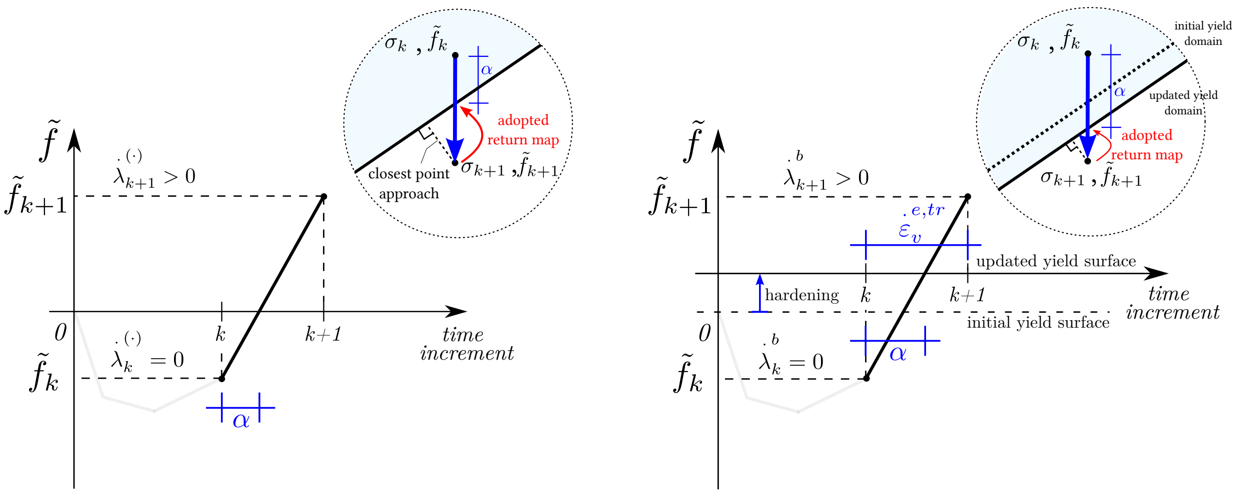

(a) unstrengthened case: mortar and units

(b) strengthened case: units

Figure 4: Graphical scheme to find the scalar α for the correction of the elastic trial predictor in the case the consistency condition is violated.

Considering the specific problem, the adopted returning map scheme is robust and allows to find an exact solution in a single step that respects the complementary conditions. It is noteworthy to raise that such simple scheme is achievable since the vertical strain-rate is corrected for the increment $k+1$, and because the solution of the system of equations is repeated for the corresponding time increment. To this aim, an history of the state and system variables must be guaranteed at least for increments k and $k+1$, which has a marginal computational cost due to the reduced number of variables of the proposed model.

4. Computational implementation details

The system of equations are solved for each time increment k considering a given vertical strain rate $\dot{\sigma}_v$. The compatibility, constitutive, and equilibrium equations are gathered in a global matrix $\mathbf{S}$ and remain linear. An iterative approach is thus precluded but a history on the state variables is required to update the global matrix of the system for each increment. In summary, a total of fifteen variables are updated for each k^{th} increment. The following quantities are evaluated:

$$\begin{cases} \text{applied vertical stress:} & \dot{\sigma}_v \\ \text{brick units:} & \dot{\varepsilon}_h^{b,e},\ \dot{\varepsilon}_v^{b},\ \dot{\sigma}_h^{b},\ \dot{\lambda}_b,\ \dot{\varepsilon}_h^{b,pl},\ \dot{\varepsilon}_v^{b,pl} \\ \text{mortar:} & \dot{\varepsilon}_h^{m,e},\ \dot{\varepsilon}_v^{m},\ \dot{\sigma}_h^{m},\ \dot{\lambda}_m,\ \dot{\varepsilon}_h^{m,pl},\ \dot{\varepsilon}_v^{m,pl} \\ \text{FRP:} & \dot{\sigma}_{FRP},\ \dot{\varepsilon}_{FRP} \end{cases} \tag{29}$$

The problem resorts on the solution of the following set of equations:

$$\mathbf{S}_k \mathbf{x}_k = \mathbf{f}_k \tag{30}$$

in which $\mathbf{S}_k$ is the global matrix of the system; $\mathbf{x}_k$ is a column vector that stores the unknown rates for the increment k; and $\mathbf{f}_k$ is the vector that controls the rate of the applied vertical strain. For the sake of computational implementation, $\mathbf{x}_k$ has been assumed to be ordered as:

$$\mathbf{x}_k^T = [\dot{\varepsilon}_h^{b,e} \quad \dot{\varepsilon}_v^{b} \quad \dot{\varepsilon}_h^{m,e} \quad \dot{\varepsilon}_v^{m} \quad \dot{\sigma}_h^{b} \quad \dot{\sigma}_h^{m} \quad \dot{\sigma}_v \quad \dot{\lambda}_b \quad \dot{\varepsilon}_h^{b,pl} \quad \dot{\varepsilon}_v^{b,pl} \quad \dot{\lambda}_m \quad \dot{\varepsilon}_h^{m,pl} \quad \dot{\varepsilon}_v^{m,pl} \quad \dot{\varepsilon}_{FRP} \quad \dot{\sigma}_{FRP}] \tag{31}$$

The global matrix $\mathbf{S}_k$ in Eq. (30) is updated for each increment and written as:

$$\mathbf{S}_k = \left[\begin{array}{c} \mathbf{A}_k \\ \hline \mathbf{B}_i \\ \hline \mathbf{M}_i \end{array}\right] \tag{32}$$

in which $\mathbf{A}$, $\mathbf{B}_i$ and $\mathbf{M}_i$ are sub-matrices of $\mathbf{S}$. Here, the sub-matrices $\mathbf{B}_i$ and $\mathbf{M}_i$ are defined according to the state of the system components, such that the former represents the brick units and the latter the mortar joints. In specific, $\mathbf{M}_i = \mathbf{M}_e$ if mortar remains elastic or $\mathbf{M}_i = \mathbf{M}_{pl}$ if in a plastic state. Similarly, $\mathbf{B}_i = \mathbf{B}_e$ if brick units remains elastic or $\mathbf{B}_i = \mathbf{B}_{pl}$ if in a plastic state. The sub-matrix $\mathbf{A}$ is independent on the system state but may change throughout the loading history due to the change on the Poisson's ratio of mortar, whose value is incrementally updated as given in Eq. (26) according to the stress state of the previous time increment.

$$\mathbf{A}_k = \begin{bmatrix} -1 & 0 & 0 & 0 & \frac{1-\nu_b}{\tilde{E}_b} & 0 & -\frac{\nu_b}{\tilde{E}_b} & 0 & 0 & 0 & 0 & 0 & 0 & 0 & -2\frac{1-\nu_b}{\tilde{E}_b}\frac{t_{FRP}}{B-2R} \\ 0 & -1 & 0 & 0 & \frac{-2\nu_b}{E_b} & 0 & \frac{1}{E_b} & 0 & 0 & 0 & 0 & 0 & 0 & 0 & \frac{-2\nu_b}{E_b}\frac{t_{FRP}}{B-2R} \\ 0 & 0 & -1 & 0 & 0 & \frac{1-\nu_m(\sigma^m_{k-1})}{E_m} & \frac{-\nu_m(\sigma^m_{k-1})}{E_m} & 0 & 0 & 0 & 0 & 0 & 0 & 0 & 0 \\ 0 & 0 & 0 & -1 & 0 & \frac{-2\nu_m(\sigma^m_{k-1})}{E_m} & \frac{1}{E_m} & 0 & 0 & 0 & 0 & 0 & 0 & 0 & 0 \\ 0 & 0 & 0 & 0 & 2HB & tB & 0 & 0 & 0 & 0 & 0 & 0 & 0 & 0 & -2t_{FRP}(2H+t) \\ 1 & 0 & 1 & 0 & 0 & 0 & 0 & 0 & 1 & 0 & 0 & 1 & 0 & 0 & 0 \\ 0 & \frac{2H}{2H+t} & 0 & \frac{t}{2H+t} & 0 & 0 & 0 & 0 & 0 & \frac{2H}{2H+t} & 0 & 0 & \frac{t}{2H+t} & 0 & 0 \\ 0 & 0 & 0 & 0 & 0 & 0 & 0 & 0 & 0 & 0 & 0 & 0 & 0 & E_{FRP} & 1 \\ 1 & 0 & 0 & 0 & 0 & 0 & 0 & 0 & 1 & 0 & 0 & 0 & 0 & 1 & 0 \end{bmatrix} \tag{33}$$

$$\mathbf{B}_e = \begin{bmatrix} 0 & 0 & 0 & 0 & 0 & 0 & 0 & 1 & 0 & 0 & 0 & 0 & 0 & 0 & 0 \\ 0 & 0 & 0 & 0 & 0 & 0 & 0 & 0 & 1 & 0 & 0 & 0 & 0 & 0 & 0 \\ 0 & 0 & 0 & 0 & 0 & 0 & 0 & 0 & 0 & 1 & 0 & 0 & 0 & 0 & 0 \end{bmatrix} \tag{34}$$

$$\mathbf{B}_{pl} = \begin{bmatrix} 0 & 0 & 0 & 0 & 0 & 0 & 0 & -\frac{\partial f}{\partial \sigma} & 1 & 0 & 0 & 0 & 0 & 0 & 0 \\ 0 & 0 & 0 & 0 & 0 & 0 & 0 & 1 & 0 & 1 & 0 & 0 & 0 & 0 & 0 \\ 0 & 0 & 0 & 0 & -\frac{\partial f}{\partial \sigma} & 0 & 1 & 0 & 0 & 0 & 0 & 0 & 0 & 0 & 0 \end{bmatrix} \tag{35}$$

$$\mathbf{M}_e = \begin{bmatrix} 0 & 0 & 0 & 0 & 0 & 0 & 0 & 0 & 0 & 0 & 1 & 0 & 0 & 0 & 0 \\ 0 & 0 & 0 & 0 & 0 & 0 & 0 & 0 & 0 & 0 & 0 & 1 & 0 & 0 & 0 \\ 0 & 0 & 0 & 0 & 0 & 0 & 0 & 0 & 0 & 0 & 0 & 0 & 1 & 0 & 0 \end{bmatrix} \tag{36}$$

$$\mathbf{M}_{pl} = \begin{bmatrix} 0 & 0 & 0 & 0 & 0 & 0 & 0 & 0 & 0 & 0 & -\frac{\partial g}{\partial \sigma} & 1 & 0 & 0 & 0 \\ 0 & 0 & 0 & 0 & 0 & 0 & 0 & 0 & 0 & 0 & 1 & 0 & 1 & 0 & 0 \\ 0 & 0 & 0 & 0 & 0 & -\frac{\partial g}{\partial \sigma} & 1 & 0 & 0 & 0 & 0 & 0 & 0 & 0 & 0 \end{bmatrix} \tag{37}$$

In the un-strengthened case and when mortar already failed, the horizontal equilibrium is sustained only by the brick units and Eq. (7) is re-written as:

$$2HB\dot{\sigma}^b_h + \dot{\sigma}_v\left(BH - \frac{\pi R^2}{3}\right)\nu_b = 0 \tag{38}$$

The column vector $\mathbf{f}_k$ defines the rate of the applied vertical strain. Similarly to the global stiffness and given as:

$$\mathbf{f}^T_k = [0\ \ 0\ \ 0\ \ 0\ \ 0\ \ 0\ \ \dot{\varepsilon}_v\ \ 0\ \ 0\ \ a\ \ 0\ \ 0\ \ b\ \ 0\ \ 0] \tag{39}$$

in which a and b are scalars whose value is also conditioned by the state of the system. If units and mortar are elastic, then $a = b = 0$; if units yielded, then $b = -\sigma_{v,k-1} + N_{\phi,m}\sigma^b_{h,(k-1)} - f_{cm}$; and if mortar yielded, then $a = -\sigma_{v,k-1} + N_{\phi,b}\sigma^b_{h,(k-1)} - f_{cb}$.

5. Numerical application and validation with experimental data

The proposed mechanistic-based model is applied to estimate the compressive strength of squared masonry columns with a periodic arrangement. The compressive strength capacity of un-strengthened and FRP strengthened columns, which are collected from the literature, are analysed.

5.1. Selected experimental works

The experimental data selected for the validation of the proposed model include the studies from Faela et al. [18], Di Ludovico et al. [31], Aiello et al. [21], Krevaikas et al. [20], and Corradi et al. [19]. These works are considered as references in the field literature [39] and were, in part, used by other researchers for validation purposes of a FE micro-model [45] and of a regression-based expression [75]. Its selection is justified since provide (i) different cross-section dimensions for the columns; (ii) different geometries and types of masonry units; (iii) different thickness for the mortar joints; (iv) different types of mortars (i.e., weak and strong mortars); and (v) different types and number of layers for the FRP laminates used in the strengthening. Although other studies could be also evaluated, it is assumed that the data gathered, which includes a total of 87 columns, allows an extensive and representative validation of the proposed model for the particular case of squared masonry columns with a periodic arrangement.

In specific, the experimental investigation of Faella et al. [18] include the response of fifty four masonry columns under compression. The specimens include squared columns made with clay bricks, with Lecce stone, and with gray and yellow tuff stones. Different dimensions for the cross-section were considered (250×250 mm^2 and 385×385 mm^2), together with different types and number of external layers for the FRP wrapping. Three different composite systems were used and referred as C (carbon), G_A (glass fibre A) and G_B (glass fibre B). A weak mortar typical of historical constructions was considered and with an average compressive strength of 1.027 MPa obtained from tests on fourteen mortar samples (coefficient of variation of 17.9%). Mortar joints were found to have in all tested cases an approximate thickness of 10 mm. The required input related with the geometric and mechanical properties of the units, mortar and composite fibres are reported in Table 1. Failure of the strengthened specimens is generally related with the tearing of the composite fibres due to stress concentration at the corners of the column.

The experimental investigation of Di Ludovico et al. [31] include the response of nine squared clay brick masonry scaled columns characterized by cross-section dimensions 260×260 mm^2 was performed. A local volcanic ash-based mortar characterized by an average compressive strength equal to 6.9 MPa was used, which is considered to be a strong mortar and a Poisson's law of Eq. (26) is assumed. Compressive tests were also performed on six orthogonal prisms of clay bricks specimens ($55 \times 115 \times 255$ mm^3) by obtaining an average value of the compressive strength equal to 22.71 MPa. Glass (GFRP) and Basalt (BFRP) FRP reinforcements were used and in the form of laminates. The following mechanical properties characterized the reinforcements: (i) BFRP with a tensile strength equal to 1814 MPa, Young's modulus equal to 91 GPa, thickness equal to 0.24mm; (i) GFRP laminate with a tensile strength 1371 MPa, Young's modulus equal to 68.74 GPa, thickness equal to 0.48 mm. The failure mode reported for the un-strengthened case is generally related with a gradual formation of longitudinal cracks in brick units that concentrated mainly at the ends of columns. In case of strengthened specimens, a brittle failure due to the rupture of the composite fibres was generally observed. The required input related with the geometric and mechanical properties of the units, mortar and composites are reported in Table 2.

The experimental investigation of Aiello et al. [21] include the response of twelve squared masonry columns made of calcareous stone (limestone) or clay bricks and with a cross-section of 250×250 mm^2. Experimental characterization tests evidenced a compressive strength of 13.61 MPa (CoV of 7.35%) for limestone masonry units and a compression strength of 23.29 MPa for clay bricks (CoV of 4.2%). The used mortar has a compressive strength of 7.80 MPa (coefficient of variation of 10.9%), thence herein classified as of a strong type and the use of the Poisson's law of Eq. (26) is considered. A thickness of 10 mm was adopted for the mortar joints of all specimens. The specimens were wrapped with one or two layers of uni-directional Glass FRP (GFRP) sheets that were bonded using an epoxy adhesive. The failure modes reported show a significant effect of the corner radius of the section. The authors found that the failure of strengthened specimens is generally associated with stress concentration at the corners and is significantly dependent on the adopted corner radius R. The required input related with the geometric and mechanical properties of the units, mortar and composites are reported in Table 3.

The experimental investigation of Krevaikas et al. [20] include the response of twelve squared masonry columns with a cross-section of 115×115 mm^2. Clay bricks with dimensions of 55×40×115 mm^3 and an average compressive strength of 23.5 MPa were used. Units were bounded by a mortar containing cement and lime as binder and at a water:cement:lime:sand ratio equal to 0.9:1:3:7.5 by weight. The 28-day compressive strength of mortar was reported as 2.85 MPa, thence classified of a strong type and the use of the Poisson's law of Eq. (26) is considered. The thickness of mortar bed joints was approximately 10 mm for all tested specimens. The specimens were were wrapped with one, two, or three layers of unidirectional Carbon FRP (CFRP) sheets or with five layers of unidirectional Glass FRP (GFRP) sheets. The mechanical properties of the fibre-polymer composite sheets was provided by the supplier. The required input related with the geometric and mechanical properties of the units, mortar and composite are reported in Table 4. In what concerns the observed failure modes, the authors reported that it was identical for all the FRP-wrapped columns. It was characterized by the onset of of vertical cracks through mortar joints and bricks that developed up to form crushed masonry, which ultimately fail by the lateral expansion that surpasses the deformation capacity of FRP.

At last, the experimental investigation of Corradi et al. [19] is considered. The response of three squared masonry columns with a cross-section of 250 × 250 mm^2 is included. Mechanical characterization tests were performed for the clay bricks, mortar and for the reinforcement (fibers and epoxy-resins). The solid clay bricks with dimensions 245 × 120 × 55 mm^3 had an average compressive strength of 20.78 MPa. The mortar was composed of Portland cement, sand and hydraulic lime with a 28-day compressive strength of 10.0 MPa. Two types of Carbon FRP (CFRP) were used, one related with high tensile fibres (HT) and other with a high Young's modulus (VHM). The required input related with the geometric and mechanical properties of the units, mortar and composites are reported in Table 5.

5.2. *Discussion of results*

The compressive strength prediction of the proposed mechanistic model are summarized in Table 1 to Table 5. Information on the geometry, on the mechanical properties of the materials, and on the typology of the used reinforcement is also reported for different compression tests on periodic masonry columns, which constitute a comprehensive literature review in the field. Assumed input values are given between curved brackets, in which an effort has been made to respect general rules of thumb. In specific, (i) a value for the Young's moduli E of units and mortar that is function of the corresponding compressive strength f_c, such that $500 f_c < E < 1000 f_c$; and (ii) a tensile strength f_t for the masonry components that is calculated as $f_t = 2.23 \log(1 + 0.075 f_c)$ according to literature recommendations [69]; (iii) an internal friction angle for units of 45 degrees; and (iv) a slope value for the Coulomb failure given as $N_{\phi_m} = 3.0$ for a 'strong' mortar and $N_{\phi_m} = 2.5$ for a 'weak' mortar (see Appendix A). Furthermore, the results are presented in Fig. 5(a)-(d) and complemented with the predictions found with Eurocode 6 [76] and ACI 530.1-02/ASCE 6-02 [77] formulas for un-strengthened columns, and with the IT CNR DT200-2004 [35] formula for strengthened columns.

Before delving in the discussion of results, it is noteworthy to briefly mention the differences among the latter normative formulas. Eurocode 6 [76] and ACI 530.1-02/ASCE 6-02 [77] provide a relationship between the compressive strength of units and mortar, which is established according to different constants that have been experimentally calibrated for different types of units and mortars. Further details are provided in Appendix B, being here recalled that these are exclusively used to evaluate the compressive strength of un-strengthened masonry columns. Differently, the IT CNR DT200-2004 [35] formula provides an empirical relationship in case of strengthening columns with FRP wrapping. It requires, however, the compressive strength of un-strengthening masonry columns (or wallets) as input (see Appendix B).

Results are given in Fig. 5 and indicate that the proposed model leads to estimations that are generally within +/-25% with the experimental data. These limits are solely added to help in the interpretation of the relative differences of the results, and do not intend to represent any statistical characteristic related with a safety factor. The results show that accurate estimations are found for clay brick masonry (Fig. 5(a),(d)) and larger deviations obtained for a tuff stone (Fig. 5(b)). Eurocode 6 [76] and ACI 530.1-02/ASCE 6-02 [77] give conservative predictions, especially evident for clay brick masonry. The IT CNR DT200-2004 [35] leads generally to estimations within the +/-25% margin and, when the latter is violated, it guarantees nonetheless a conservative estimation. Yet, a closer look on the samples for which the proposed model tends to be outside the deviation fork of +/-25% allows to conclude that the material uncertainty may play an important role. Results of Fig. 5 are obtained considering the mean strength values for the components characterization tests reported in each study, but it is clear that significant standard deviations were found as demonstrated in Table 6.

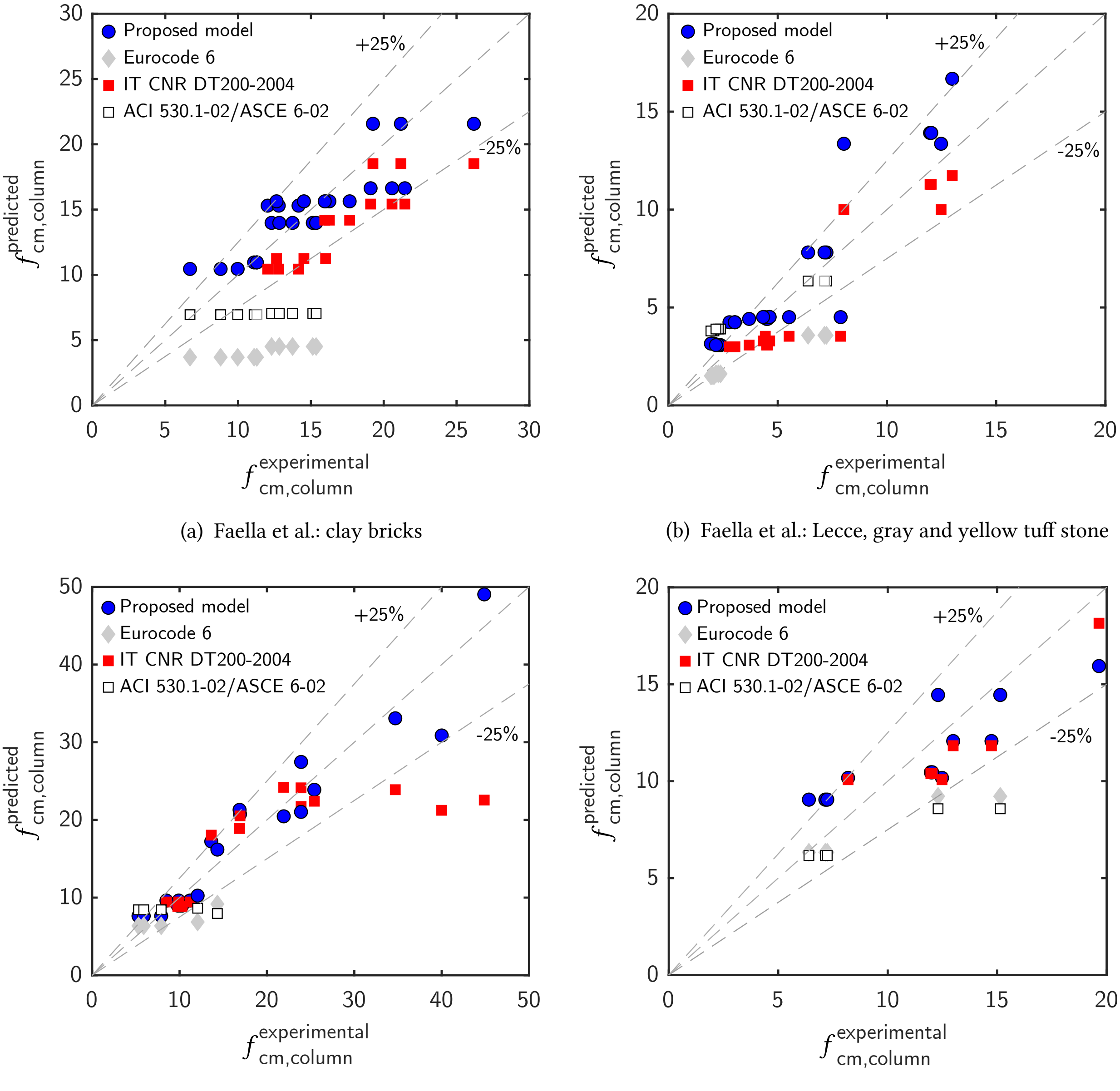

(a) Faella et al.: clay bricks

(b) Faella et al.: Lecce, gray and yellow tuff stone

(c) Di Ludovico et al., Krevaikas et al. and Corradi et al.: clay bricks

(d) Aiello et al.: limestone and clay bricks

Figure 5: Comparison between the proposed model and normative-based formulas.

In order to explore the effect of material uncertainty, it is decided to conduct the analyses by considering that the experimental input data follows a normal distribution and for a 99.87% confidence level. In specific, the compressive and tensile strength values for units and mortar have a lower and an upper limit that lies three standard deviations from the reported mean value. Exception is made for the Lecce, grey and yellow tuff stones [18], in which the minimum and maximum strength input values for mortar and units are available from the experiments and assumed. The relative differences between the predicted and the experimental value are given for the un-strengthened and strengthened cases in Fig. 6.

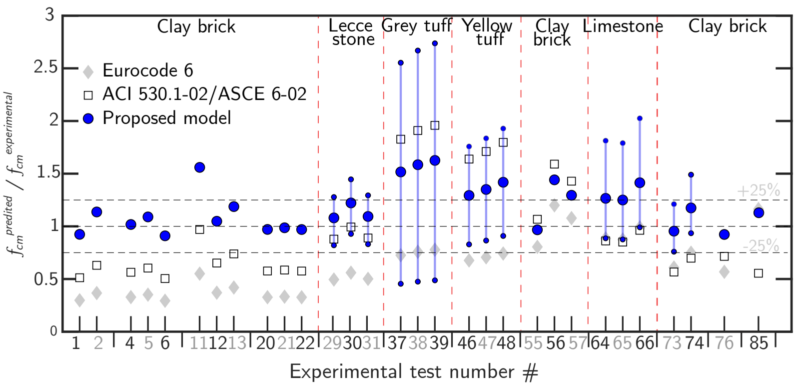

(a) un-strengthened masonry columns

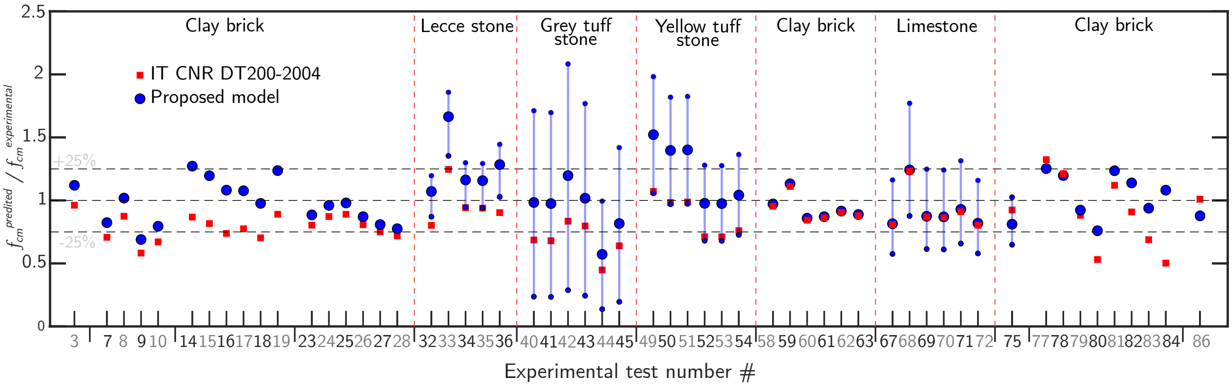

(b) strengthened masonry columns

Figure 6: Comparison between the proposed model and normative-based formulas.

Regarding the former case in Fig. 6(a), the proposed model shows the lowest differences with the experimental data, whereas the normatives appear to be generally conservative. However, two remarks are noteworthy. Firstly, it can be addressed that the Eurocode formula does not follow a particular trend. The recommended value of $K = 0.55$ (see Appendix B) seems too low since it leads to differences higher than 50% for clay brick columns #3 – #28 [18]. A different conclusion is found for the clay brick columns #3 – #28 of Di Ludovico et al. [31] with non-conservative strength estimations. Secondly, the results from ACI exhibit in most of the cases a lower bond solution that tends to be within a 25% to 50% difference, but which evidences non-conservative estimations for the samples with a significant material uncertainty (grey tuff stone, yellow tuff stone and limestone).

For the strengthened columns, the Italian code provides conservative results but, nonetheless, some accurate predictions are observed for limestone and clay masonry, in which an overlapping with the proposed model is found for samples #56 and #57 (Fig.6(b)). A lower scattering is found for both approaches in the clay brick columns. This is somehow aligned with the experimental observations as a more consistent failure has been found. Differently, and as concluded from Fig. 5, the deviations are higher for the grey tuff stone, yellow tuff stone and limestone. Nonetheless, the experimental value lies within the box plots corresponding to a 99.87% of data for the proposed model. The material uncertainty can, therefore, justify such deviations.

Table 1: Input data and results according to the experiments from Faella et al. [18] (assumed values between curved brackets).

Test	Code	Masonry prism					Units			Mortar	Strengthening			Mechanical properties for brick units				Mechanical properties for mortar				Reinforcement		Compressive strength	
		B (mm)	D (mm)	h (mm)	R (mm)	type	h (mm)	b (mm)	L (mm)	t (mm)	FRP type	n. layers	t_{eq} (mm)	E_b (MPa)	ν_b (-)	f_{cb} (MPa)	f_{tb} (MPa)	E_m (MPa)	ν_m (-)	f_{cm} (MPa)	f_{tm} (MPa)	E_{FRP} (MPa)	$f_{t,FRP}$ (MPa)	f_m^{exp} (MPa)	$f_m^{proposed}$ (MPa)
1	B#19UR	250	250	500	10		30	120	250	10	-	-	-	{20000}	{0.15}	20.0	{1.95}	{1000}	{0.3}	1.027	0.1573 [69]	-	-	15.13	13.98
2	B#20UR	250	250	500	10		30	120	250	10	-	-	-	{20000}	{0.15}	20.0	1.95 [69]	{1000}	{0.3}	1.027	0.1573 [69]	-	-	12.30	13.98
3	B#21G1	250	250	500	10		30	120	250	10	Ga	1	0.48	{20000}	{0.15}	20.0	1.95 [69]	{1000}	{0.3}	1.027	0.1573 [69]	80700	2560	19.26	21.57
4	B#22UR	250	250	500	10		30	120	250	10	-	-	-	{20000}	{0.15}	20.0	1.95 [69]	{1000}	{0.3}	1.027	0.1573 [69]	-	-	13.74	13.98
5	B#23UR	250	250	500	10	Clay brick type A	30	120	250	10	-	-	-	{20000}	{0.15}	20.0	1.95 [69]	{1000}	{0.3}	1.027	0.1573 [69]	-	-	12.83	13.98
6	B#24UR	250	250	500	10		30	120	250	10	-	-	-	{20000}	{0.15}	20.0	1.95 [69]	{1000}	{0.3}	1.027	0.1573 [69]	-	-	15.36	13.98
7	B#25G1	250	250	500	10		30	120	250	10	Ga	1	0.48	{20000}	{0.15}	20.0	1.95 [69]	{1000}	{0.3}	1.027	0.1573 [69]	80700	2560	26.19	21.57
8	B#26G1	250	250	500	10		30	120	250	10	Ga	1	0.48	{20000}	{0.15}	20.0	1.95 [69]	{1000}	{0.3}	1.027	0.1573 [69]	80700	2560	21.18	21.57
9	B#27G2	250	250	500	10		30	120	250	10	Ga	2	0.96	{20000}	{0.15}	20.0	1.95 [69]	{1000}	{0.3}	1.027	0.1573 [69]	80700	2560	35.13	24.22
10	B#28G2	250	250	500	10		30	120	250	10	Ga	2	0.96	{20000}	{0.15}	20.0	1.95 [69]	{1000}	{0.3}	1.027	0.1573 [69]	80700	2560	30.48	24.22
11	B#01UR	372	371	489	25		55	120	250	10	-	-	-	{15000}	{0.15}	15.0	1.59 [69]	{1000}	{0.3}	1.027	0.1573 [69]	-	-	6.70	10.45
12	B#02UR	377	378	499	25		55	120	250	10	-	-	-	{15000}	{0.15}	15.0	1.59 [69]	{1000}	{0.3}	1.027	0.1573 [69]	-	-	9.97	10.45
13	B#03UR	371	371	487	25		55	120	250	10	-	-	-	{15000}	{0.15}	15.0	1.59 [69]	{1000}	{0.3}	1.027	0.1573 [69]	-	-	8.80	10.45
14	B#04G1	380	383	492	25		55	120	250	10	Gb	1	0.23	{15000}	{0.15}	15.0	1.59 [69]	{1000}	{0.3}	1.027	0.1573 [69]	65000	1600	12.03	15.30
15	B#05G1	387	375	485	25		55	120	250	10	Gb	1	0.23	{15000}	{0.15}	15.0	1.59 [69]	{1000}	{0.3}	1.027	0.1573 [69]	65000	1600	12.79	15.30
16	B#06G1	377	380	488	25		55	120	250	10	Gb	1	0.23	{15000}	{0.15}	15.0	1.59 [69]	{1000}	{0.3}	1.027	0.1573 [69]	65000	1600	14.15	15.30
17	B#07G2	383	378	486	25		55	120	250	10	Gb	2	0.46	{15000}	{0.15}	15.0	1.59 [69]	{1000}	{0.3}	1.027	0.1573 [69]	65000	1600	14.52	15.63
18	B#08G2	377	378	481	25		55	120	250	10	Gb	2	0.46	{15000}	{0.15}	15.0	1.59 [69]	{1000}	{0.3}	1.027	0.1573 [69]	65000	1600	16.01	15.63
19	B#09G2	383	374	492	25	Clay brick type B	55	120	250	10	Gb	2	0.46	{15000}	{0.15}	15.0	1.59 [69]	{1000}	{0.3}	1.027	0.1573 [69]	65000	1600	12.64	15.63
20	B#10UR	240	248	472	25		55	120	250	10	-	-	-	{15000}	{0.15}	15.0	1.59 [69]	{1000}	{0.3}	1.027	0.1573 [69]	-	-	11.28	10.95
21	B#11UR	243	244	477	25		55	120	250	10	-	-	-	{15000}	{0.15}	15.0	1.59 [69]	{1000}	{0.3}	1.027	0.1573 [69]	-	-	11.10	10.95
22	B#12UR	243	245	474	25		55	120	250	10	-	-	-	{15000}	{0.15}	15.0	1.59 [69]	{1000}	{0.3}	1.027	0.1573 [69]	-	-	11.29	10.95
23	B#13G1	250	248	470	25		55	120	250	10	Gb	1	0.23	{15000}	{0.15}	15.0	1.59 [69]	{1000}	{0.3}	1.027	0.1573 [69]	65000	1600	17.66	15.63
24	B#14G1	250	249	470	25		55	120	250	10	Gb	1	0.23	{15000}	{0.15}	15.0	1.59 [69]	{1000}	{0.3}	1.027	0.1573 [69]	65000	1600	16.27	15.63
25	B#15G1	250	247	470	25		55	120	250	10	Gb	1	0.23	{15000}	{0.15}	15.0	1.59 [69]	{1000}	{0.3}	1.027	0.1573 [69]	65000	1600	15.95	15.63
26	B#16G2	248	247	462	25		55	120	250	10	Gb	2	0.46	{15000}	{0.15}	15.0	1.59 [69]	{1000}	{0.3}	1.027	0.1573 [69]	65000	1600	19.10	16.63
27	B#17G2	245	248	471	25		55	120	250	10	Gb	2	0.46	{15000}	{0.15}	15.0	1.59 [69]	{1000}	{0.3}	1.027	0.1573 [69]	65000	1600	20.57	16.63
28	B#18G2	246	251	473	25		55	120	250	10	Gb	2	0.46	{15000}	{0.15}	15.0	1.59 [69]	{1000}	{0.3}	1.027	0.1573 [69]	65000	1600	21.45	16.63
29	L#01UR	250	250	500	0		30	120	250	10	-	-	-	{14370}	{0.25}	14.37	1.55 [69]	{1000}	{0.3}	1.027	0.1573 [69]	-	-	7.23	7.81
30	L#02UR	250	250	500	0		30	120	250	10	-	-	-	{14370}	{0.25}	14.37	1.55 [69]	{1000}	{0.3}	1.027	0.1573 [69]	-	-	6.39	7.81
31	L#03UR	250	250	500	0		30	120	250	10	-	-	-	{14370}	{0.15}	14.37	1.55 [69]	{1000}	{0.3}	1.027	0.1573 [69]	-	-	7.14	7.81
32	L#04G1	250	250	500	10	Lecce stone	30	120	250	10	Ga	1	0.48	{14370}	{0.25}	14.37	1.55 [69]	{1000}	{0.3}	1.027	0.1573 [69]	80700	2560	12.48	13.36
33	L#05G1	250	250	500	10		30	120	250	10	Ga	1	0.48	{14370}	{0.25}	14.37	1.55 [69]	{1000}	{0.3}	1.027	0.1573 [69]	80700	2560	8.03	13.36
34	L#06G1	250	250	500	20		30	120	250	10	Ga	1	0.48	{14370}	{0.25}	14.37	1.55 [69]	{1000}	{0.3}	1.027	0.1573 [69]	80700	2560	11.97	13.91
35	L#07G1	250	250	500	20		30	120	250	10	Ga	1	0.48	{14370}	{0.25}	14.37	1.55 [69]	{1000}	{0.3}	1.027	0.1573 [69]	80700	2560	12.03	13.91
36	L#08G2	250	250	500	20		30	120	250	10	Ga	2	0.96	{14370}	{0.25}	14.37	1.55 [69]	{1000}	{0.3}	1.027	0.1573 [69]	80700	2560	12.99	16.67
37	T#01UR	395	395	525	25		120	250	120	10	–	–	–	{4200}	{0.15}	4.20	0.58 [69]	{1000}	{0.3}	1.027	0.1573 [69]	-	-	2.08	3.15
38	T#02UR	388	393	509	25		120	250	120	10	–	–	–	{4200}	{0.15}	4.20	0.58 [69]	{1000}	{0.3}	1.027	0.1573 [69]	-	-	1.99	3.15
39	T#03UR	392	387	500	25		120	250	120	10	–	–	–	{4200}	{0.15}	4.20	0.58 [69]	{1000}	{0.3}	1.027	0.1573 [69]	-	-	1.94	3.15
40	T#04C1	389	391	499	25		120	250	120	10	C	1	0.167	{4200}	{0.15}	4.20	0.58 [69]	{1000}	{0.3}	1.027	0.1573 [69]	230000	3400	4.49	4.41
41	T#05C1	403	397	499	25	Grey tuff stone	120	250	120	10	C	1	0.167	{4200}	{0.15}	4.20	0.58 [69]	{1000}	{0.3}	1.027	0.1573 [69]	230000	3400	4.53	4.41
42	T#06C1	397	393	486	25		120	250	120	10	C	1	0.167	{4200}	{0.15}	4.20	0.58 [69]	{1000}	{0.3}	1.027	0.1573 [69]	230000	3400	3.69	4.41
43	T#07C1	386	394	500	25		120	250	120	10	C	2	0.334	{4200}	{0.15}	4.20	0.58 [69]	{1000}	{0.3}	1.027	0.1573 [69]	230000	3400	4.43	4.51
44	T#08C2	392	393	492	25		120	250	120	10	C	2	0.334	{4200}	{0.15}	4.20	0.58 [69]	{1000}	{0.3}	1.027	0.1573 [69]	230000	3400	7.88	4.51
45	T#09C2	394	386	511	25		120	250	120	10	C	2	0.334	{4200}	{0.15}	4.20	0.58 [69]	{1000}	{0.3}	1.027	0.1573 [69]	230000	3400	5.52	4.51
46	T#10UR	382	399	479	25		120	250	120	10	–	–	–	{4600}	{0.15}	4.06	0.56 [69]	{1000}	{0.3}	1.027	0.1573 [69]	–	–	2.38	3.08
47	T#11UR	381	400	477	25		120	250	120	10	–	–	–	{4600}	{0.15}	4.06	0.56 [69]	{1000}	{0.3}	1.027	0.1573 [69]	–	–	2.28	3.08
48	T#12UR	392	394	492	25		120	250	120	10	–	–	–	{4600}	{0.15}	4.06	0.56 [69]	{1000}	{0.3}	1.027	0.1573 [69]	–	–	2.17	3.08
49	T#13G1	398	400	503	25		120	250	120	10	GB	1	0.23	{4600}	{0.15}	4.06	0.56 [69]	{1000}	{0.3}	1.027	0.1573 [69]	65000	1600	2.79	4.25
50	T#14G1	400	400	490	25	Yellow tuff stone	120	250	120	10	GB	1	0.23	{4600}	{0.15}	4.06	0.56 [69]	{1000}	{0.3}	1.027	0.1573 [69]	65000	1600	3.04	4.25
51	T#15G1	400	388	485	25		120	250	120	10	GB	1	0.23	{4600}	{0.15}	4.06	0.56 [69]	{1000}	{0.3}	1.027	0.1573 [69]	65000	1600	3.03	4.25
52	T#16G2	394	389	505	25		120	250	120	10	GB	2	0.46	{4600}	{0.15}	4.06	0.56 [69]	{1000}	{0.3}	1.027	0.1573 [69]	65000	1600	4.62	4.51
53	T#17G2	402	405	486	25		120	250	120	10	GB	2	0.46	{4600}	{0.15}	4.06	0.56 [69]	{1000}	{0.3}	1.027	0.1573 [69]	65000	1600	4.63	4.51
54	T#18G2	395	392	480	25		120	250	120	10	GB	2	0.46	{4600}	{0.15}	4.06	0.56 [69]	{1000}	{0.3}	1.027	0.1573 [69]	65000	1600	4.33	4.51

Table 2: Input data and results according to the experiments from Di Ludovico et al. [31] (assumed values between curved brackets).

Test	Code	Masonry prism					Units			Mortar	Strengthening			Mechanical properties for brick units				Mechanical properties for mortar				Reinforcement		Compressive strength	
		B (mm)	D (mm)	h (mm)	R (mm)	type	h (mm)	b (mm)	L (mm)	t (mm)	FRP type	n. layers	t_{eq} (mm)	E_b (MPa)	ν_b (-)	f_{cb} (MPa)	f_{tb} (MPa)	E_m (MPa)	ν_m (-)	f_{cm} (MPa)	f_{tm} (MPa)	E_{FRP} (MPa)	$f_{t,FRP}$ (MPa)	f_m^{exp} (MPa)	$f_m^{proposed}$ (MPa)
55	B-U-1	259	260	560	20		55	115	255	12	-	-	-	{15000}	0.15	22.71	$\{f_{cb}/50\}$	{6900}	{0.3}	6.9	1.71 [69]	-	-	7.90	7.64
56	B-U-2	259	257	575	20	Clay brick	55	115	255	12	-	-	-	{15000}	0.15	22.71	$\{f_{cb}/50\}$	{6900}	{0.3}	6.9	1.71 [69]	-	-	5.30	7.64
57	B-U-3	260	258	560	20		55	115	255	12	-	-	-	{15000}	0.15	22.71	$\{f_{cb}/50\}$	{6900}	{0.3}	6.9	1.71 [69]	-	-	5.90	7.64
58	B-G-1	264	265	560	20		55	115	255	12	G	1	0.48	{15000}	0.15	22.71	$\{f_{cb}/50\}$	{6900}	{0.3}	6.9	1.71 [69]	68740	1371	9.90	9.62
59	B-G-2	267	265	560	20	Clay brick	55	115	255	12	G	1	0.48	{15000}	0.15	22.71	$\{f_{cb}/50\}$	{6900}	{0.3}	6.9	1.71 [69]	68740	1371	8.50	9.62
60	B-G-3	266	265	560	20		55	115	255	12	G	1	0.48	{15000}	0.15	22.71	$\{f_{cb}/50\}$	{6900}	{0.3}	6.9	1.71 [69]	68740	1371	11.20	9.62
61	B-B-1	266	266	560	20		55	115	255	12	B	1	0.24	{15000}	0.15	22.71	$\{f_{cb}/50\}$	{6900}	{0.3}	6.9	1.71 [69]	91000	1814	10.30	8.97
62	B-B-2	265	264	560	20	Clay brick	55	115	255	12	B	1	0.24	{15000}	0.15	22.71	$\{f_{cb}/50\}$	{6900}	{0.3}	6.9	1.71 [69]	91000	1814	9.80	8.97
63	B-B-3	265	264	560	20		55	115	255	12	B	1	0.24	{15000}	0.15	22.71	$\{f_{cb}/50\}$	{6900}	{0.3}	6.9	1.71 [69]	91000	1814	10.10	8.97

Table 3: Input data and results according to the experiments from Aiello et al. [21] (assumed values between curved brackets).

Test	Code	Masonry prism					Units			Mortar	Strengthening			Mechanical properties for brick units				Mechanical properties for mortar				Reinforcement		Compressive strength	
		B (mm)	D (mm)	h (mm)	R (mm)	type	h (mm)	b (mm)	L (mm)	t (mm)	FRP type	n. layers	t_{eq} (mm)	E_b (MPa)	ν_b (-)	f_{cb} (MPa)	f_{tb} (MPa)	E_m (MPa)	ν_m (-)	f_{cm} (MPa)	f_{tm} (MPa)	E_{FRP} (MPa)	$f_{t,FRP}$ (MPa)	f_m^{exp} (MPa)	$f_m^{proposed}$ (MPa)
64	SFC-1	250	250	500	-		30	125	250	10	-			{13610}	{0.15}	13.61	1.49 [69]	{3500}	{0.3}	7.80	0.97 [69]	-	-	7.15	9.05
65	SFC-2	250	250	500	-		30	125	250	10	-			{13610}	{0.15}	13.61	1.49 [69]	{3500}	{0.3}	7.80	0.97 [69]	-	-	7.24	9.05
66	SFC-3	250	250	500	-		30	125	250	10	-			{13610}	{0.15}	13.61	1.49 [69]	{3500}	{0.3}	7.80	0.97 [69]	-	-	6.40	9.05
67	SFW-R1-1	250	250	500	10		30	125	250	10	G	1	0.48	{13610}	{0.15}	13.61	1.49 [69]	{3500}	{0.3}	7.80	0.97 [69]	74143	1605	12.48	10.17
68	SFW-R1-2	250	250	500	10	Limestone	30	125	250	10	G	1	0.48	{13610}	{0.15}	13.61	1.49 [69]	{3500}	{0.3}	7.80	0.97 [69]	74143	1605	8.19	10.17
69	SFW-R2-1	250	250	500	20		30	125	250	10	G	1	0.48	{13610}	{0.15}	13.61	1.49 [69]	{3500}	{0.3}	7.80	0.97 [69]	74143	1605	11.97	10.46
70	SFW-R2-2	250	250	500	20		30	125	250	10	G	1	0.48	{13610}	{0.15}	13.61	1.49 [69]	{3500}	{0.3}	7.80	0.97 [69]	74143	1605	12.03	10.46
71	SFW2-R2-1	250	250	500	20		30	125	250	10	G	2	0.96	{13610}	{0.15}	13.61	1.49 [69]	{3500}	{0.3}	7.80	0.97 [69]	74143	1605	12.99	12.07
72	SFW2-R2-2	250	250	500	20		30	125	250	10	G	2	0.96	{13610}	{0.15}	13.61	1.49 [69]	{3500}	{0.3}	7.80	0.97 [69]	74143	1605	14.74	12.07
73	LC-1	250	250	500	—		30	125	250	10	-	-	-	{20000}	{0.10}	23.29	1.49 [69]	{3500}	{0.3}	7.80	0.97 [69]	74143	1605	15.14	14.45
74	LC-2	250	250	500	—	Clay brick	30	125	250	10	-	-	-	{20000}	{0.10}	23.29	1.49 [69]	{3500}	{0.3}	7.80	0.97 [69]	74143	1605	12.3	14.45
75	LW-R1	250	250	500	10		30	125	250	10	G	1	0.48	{20000}	{0.10}	23.29	1.49 [69]	{3500}	{0.3}	7.80	0.97 [69]	74143	1605	19.65	15.94

Table 4: Input data and results according to the experiments from Krevaikas et al. [20] (assumed values between curved brackets).

Test	Code	Masonry prism					Units			Mortar	Strengthening			Mechanical properties for brick units				Mechanical properties for mortar				Reinforcement		Compressive strength	
		B (mm)	D (mm)	h (mm)	R (mm)	type	h (mm)	b (mm)	L (mm)	t (mm)	FRP type	n. layers	t_{eq} (mm)	E_b (MPa)	ν_b (-)	f_{cb} (MPa)	f_{tb} (MPa)	E_m (MPa)	ν_m (-)	f_{cm} (MPa)	f_{tm} (MPa)	E_{FRP} (MPa)	$f_{t,FRP}$ (MPa)	f_m^{exp} (MPa)	$f_m^{proposed}$ (MPa)
76	C0_1_R10	115	115	340	10		40.00	55	115	10	-	-	-	{16000}	{0.17}	23.50	2.15 [69]	{1000}	{0.30}	2.85	0.41 [69]	-	-	12.07	10.25
77	C1_1_R10	115	115	340	10		40	55	115	10	C	1	0.118	{16000}	{0.17}	23.50	2.15 [69]	{1000}	{0.30}	2.85	0.41 [69]	230000	3500	13.63	17.23
78	C2_1_R10	115	115	340	10		40	55	115	10	C	2	0.236	{16000}	{0.17}	23.50	2.15 [69]	{1000}	{0.30}	2.85	0.41 [69]	230000	3500	16.92	20.75
79	C3_1_R10	115	115	340	10		40	55	115	10	C	3	0.354	{16000}	{0.17}	23.50	2.15 [69]	{1000}	{0.30}	2.85	0.41 [69]	230000	3500	25.42	23.88
80	G5_1_R10	115	115	340	10	Clay brick	40	55	115	10	G	5	0.915	{16000}	{0.17}	23.50	2.15 [69]	{1000}	{0.30}	2.85	0.41 [69]	70000	2000	40	30.87
81	C1_1_R20	115	115	340	20		40	55	115	10	C	1	0.118	{16000}	{0.17}	23.50	2.15 [69]	{1000}	{0.30}	2.15	0.32 [69]	230000	3500	16.87	21.30
82	C2_1_R20	115	115	340	20		40	55	115	10	C	2	0.118	{16000}	{0.17}	23.50	2.15 [69]	{1000}	{0.30}	2.15	0.32 [69]	230000	3500	23.91	27.46
83	C3_1_R20	115	115	340	20		40	55	115	10	C	3	0.118	{16000}	{0.17}	23.50	2.15 [69]	{1000}	{0.30}	2.15	0.32 [69]	230000	3500	34.69	33.08
84	G5_1_R20	115	115	340	20		40	55	115	10	G	5	0.183	{16000}	{0.17}	23.50	2.15 [69]	{1000}	{0.30}	2.15	0.32 [69]	70000	2000	44.87	49.03

Table 5: Input data and results according to the experiments from Corradi et al. [19] (assumed values between curved brackets).

Test	Code	Masonry prism					Units			Mortar	Strengthening			Mechanical properties for brick units				Mechanical properties for mortar				Reinforcement		Compressive strength	
		B (mm)	D (mm)	h (mm)	R (mm)	type	h (mm)	b (mm)	L (mm)	t (mm)	FRP type	n. layers	t_{eq} (mm)	E_b (MPa)	ν_b (-)	f_{cb} (MPa)	f_{tb} (MPa)	E_m (MPa)	ν_m (-)	f_{cm} (MPa)	f_{tm} (MPa)	E_{FRP} (MPa)	$f_{t,FRP}$ (MPa)	f_m^{exp} (MPa)	$f_m^{proposed}$ (MPa)
85	Un-confined	245	250	500	-	Clay brick	55	120	245	8	-	-	-	{20780}	{0.10}	20.78	1.99 [69]	{10000}	{0.30}	10.0	1.19 [69]	-	-	14.33	16.18
86	S-HT-2	245	250	500	20		55	120	245	8	C	2	0.165	{20780}	{0.10}	20.78	1.99 [69]	{10000}	{0.30}	10.0	1.19 [69]	417625	3388	23.90	21.03
87	S-VHM-2	245	250	500	20		55	120	245	8	C	2	0.143	{20780}	{0.10}	20.78	1.99 [69]	{10000}	{0.30}	10.0	1.19 [69]	673200	1955	21.92	20.46

Table 6: Literature data from the experimental characterization tests on the masonry components (n/a: not available).

<table>
<tr><th>Reference study</th><th>Test number #</th><th>f_{cb} (MPa)</th><th>SD (f_{cb}) (MPa)</th><th>f_{cm} (MPa)</th><th>SD (f_{cm}) (MPa)</th></tr>
<tr><td>Faella et al.[18] (clay brick type A)</td><td>1-10</td><td>n/a</td><td>n/a</td><td rowspan="5">1.027 ('weak' mortar)</td><td rowspan="5">0.184</td></tr>
<tr><td>Faella et al.[18] (clay brick type B)</td><td>10-28</td><td>n/a</td><td>n/a</td></tr>
<tr><td>Faella et al.[18] (Lecce stone)</td><td>29-36</td><td>14.37</td><td>2.40</td></tr>
<tr><td>Faella et al.[18] (Grey tuff stone)</td><td>27-45</td><td>4.20</td><td>2.28</td></tr>
<tr><td>Faella et al.[18] (Yellow tuff stone)</td><td>46-54</td><td>4.06</td><td>0.42</td></tr>
<tr><td>Di Ludovico et al.[31] (clay brick)</td><td>55-63</td><td>22.71</td><td>n/a</td><td>6.90 ('strong' mortar)</td><td>n/a</td></tr>
<tr><td>Aiello et al.[21] (limestone)</td><td>64-72</td><td>13.61</td><td>1.00</td><td rowspan="2">7.80 ('strong' mortar)</td><td rowspan="2">0.85</td></tr>
<tr><td>Aiello et al.[21] (clay brick)</td><td>73-75</td><td>23.29</td><td>1.00</td></tr>
<tr><td>Krevaikas et al.[20] (clay brick 1st series)</td><td>76-80</td><td>23.5</td><td>n/a</td><td>2.85 ('strong' mortar)</td><td>n/a</td></tr>
<tr><td>Krevaikas et al.[20] (clay brick 2nd series)</td><td>81-84</td><td>23.5</td><td>n/a</td><td>2.15 ('strong' mortar)</td><td>n/a</td></tr>
<tr><td>Corradi et al.[19] (clay brick)</td><td>85-87</td><td>20.78</td><td>n/a</td><td>10.0 ('strong' mortar)</td><td>n/a</td></tr>
</table>

6. Conclusions

A mechanistic model was proposed for the evaluation of the compressive strength of non-strenghened and FRP-strengthened masonry squared columns. It addresses the main gap identified in the literature [33, 39], i.e. to establish a predictive model that precludes the knowledge of the unconfined (un-strengthened) compressive strength of the masonry and that stems directly from hypotheses related with the mechanical behaviour of the masonry components, thence by-passing the use of concrete-related expressions as reference. We are bounded by the following hypotheses: (i) the masonry has a periodic arrangement, (ii) the masonry column has a squared transversal section; and (iii) the retrofitting is based on a fibre-polymer composite wrapping technique.

The model stands on Hilsdorf's assumptions for the response of masonry under compression, however improved to include (i) the elasto-plastic behaviour of units and mortar joints; (ii) the non-linear elastic response of mortar due to the change of its Poisson's ratio according to the tri-axial compression state; (iii) failure of the units and mortar joints according to a multi-surface failure domain with either an associated and non-associated plastic flow rule; and (iv) an elastic response with a brittle failure for the composite wrap. The input variables of such non-conventional elasto-plastic approach are reduced and the computational implementation straightforward. The predicted compressive strength is therefore immediately available to any practitioner interested in a fast and reliable prediction of the strength in absence and presence of wrapping.

The main advantages in respect to existing normative formulas were demonstrated and are twofold: (i) a more accurate prediction of the average mechanical behaviour at failure of the columns is obtained, for which material uncertainty can be included; and (ii) it requires exclusively the elastic and failure properties of bricks, mortar and FRP, which are available in literature or found through simple characterization tests. The model competes favourably with existing formulas provided by national and international codes – typically with a phenomenological base – when applied in the prediction of the experimental compressive strength of columns reinforced in different ways and made with different typologies of blocks. A feasible evolution of the model is to consider strengthening made with inorganic matrices, such as FRCM.

Appendix A. Literature data for the mortar Coulomb failure envelope $\sigma_1 - \sigma_3$ in tri-axial compression

According to the data found by *Barbosa et al.* [43] for different mortar types (cement/lime/sand):

$$\begin{cases} \text{Type:} \quad 1:0.25:3 & \sigma_1 = f_c + 1.6\sigma_3 \\ \qquad\quad\;\; 1:0.50:4.5 & \sigma_1 = f_c + 3.2\sigma_3 \\ \qquad\quad\;\; 1:0.25:3 & \sigma_1 = f_c + 0.7\sigma_3 \end{cases} \tag{A.1}$$

According to the data found by *Atkinson et al.* [78] for different mortar types (cement/lime/sand):

$$\begin{cases} \text{Type:} \quad 1:0.25:3 \quad (W/C = 0.55) \qquad \sigma_1 = f_c + 5\sigma_3 \\ \qquad\quad 1:0.5:4.5 \quad (W/C = 0.85) \qquad \sigma_1 = f_c + 3\sigma_3 \\ \qquad\quad 1:1:6 \quad (W/C = 1.19) \qquad \sigma_1 = f_c + 2\sigma_3 \\ \qquad\quad 1:2:9 \quad (W/C = 1.96) \qquad \sigma_1 = f_c + 2\sigma_3 \end{cases} \tag{A.2}$$

According to the data found by *McNary and Abrams* [12] for different mortar types (cement/lime/sand):

$$\begin{cases} \text{Type:} \quad 1:0.25:3 \qquad \sigma_1 = f_c + 3\sigma_3 \\ \qquad\quad 1:0.5:4.5 \qquad \sigma_1 = f_c + 3.5\sigma_3 \\ \qquad\quad 1:1:6 \qquad \sigma_1 = f_c + 2.3\sigma_3 \\ \qquad\quad 1:2:9 \qquad \sigma_1 = f_c + 2.2\sigma_3 \end{cases} \tag{A.3}$$

According to the data found by *Mohamad et al.* [47] for different mortar types (cement/lime/sand):

$$\begin{cases} \text{Type:} \quad 1:0.25:3 \qquad \sigma_1 = f_c + 4\sigma_3 \\ \qquad\quad 1:0.5:4.5 \qquad \sigma_1 = f_c + 3.6\sigma_3 \\ \qquad\quad 1:1:6 \qquad \sigma_1 = f_c + 2.6\sigma_3 \\ \qquad\quad 1:2:9 \qquad \sigma_1 = f_c + 2.5\sigma_3 \end{cases} \tag{A.4}$$

Appendix B. Compressive strength prediction of masonry according to code-based analytical formulas

Appendix B.1. Eurocode 6 formula for unconfined masonry

The expression proposed by the Eurocode 6 [76] for the prediction of the compressive strength of un-strengthened masonry elements is given in Eq.(B.1):

$$f_{cM} = K f_{cb}^{\alpha} f_{cm}^{\beta} \tag{B.1}$$

in which f_{cM} (MPa) is the compressive strength of the masonry, f_{cb} (MPa) is the compressive strength of the units, f_{cm} (MPa) is the compressive strength of the mortar and K, α and β are constants. It is noteworthy to recall that f_{cM} corresponds to a mean value, as the strength parameters for brick units (f_{cb}) and mortar joints (f_{cm}) provided by the experimental data are mean values [69]. Additionally, a unitary safety factor is adopted, and the obtained values are thus less conservative than the characteristic one. General values for K are provided in the code according to the type of masonry blocks and on the characteristics of mortar. Herein, a value of $K = 0.55$ is adopted; which is associated with a clay brick masonry with a regular mortar. The recommended values for the remaining constants are adopted, i.e. $\alpha = 0.7$ and $\beta = 0.3$.

Appendix B.2. ACI 530.1-02/ASCE 6-02 for unconfined masonry

In what concerns the ACI 530.1-02/ASCE 6-02 [77], the formula presented for the calculation of the compressive strength of unconfined masonry elements is given in Eq.(B.2):

$$f_{ck} = \frac{A(400 + 145.038 B f_{bc})}{145.038} \tag{B.2}$$

in which f_{ck} (MPa) is the characteristic compressive strength of the masonry, and $A = 1$ and $B = 0.25$ (assumed for a type S or M Portland Cement-lime mortar) and f_{bc} is the compressive strength of brick units.

Appendix B.3. Italian code CNR-DT200

Lastly, the formula proposed by the Italian code CNR-DT200 for the evaluation of the design compressive strength f_{mcd} of masonry elements confined with FRP and subjected to a lateral confining pressure is given in Eq.(B.2):

$$f_{cmd} = f_{md}\Big[1 + k'\Big(\frac{f_{l,eff}}{f_{md}}\Big)^{\alpha_1}\Big] \quad , \quad k' = \alpha_2\Big(\frac{\gamma_m}{1000}\Big)^{\alpha_3} \tag{B.3}$$

in which f_{md} is the design compressive strength of unconfined masonry; α_1, α_2 and α_3 are constants and assumed as $\alpha_1 = 0.5$ and $\alpha_2 = \alpha_3 = 1.0$; γ_m is the mass density of the masonry in kg/m^3. The effective confinement pressure $f_{l,eff}$ can, assuming a squared column with cross-section dimension B and corner radius R, be evaluated as:

$$f_{l,eff} = k_H k_v f_l, \quad k_H = 1 - \frac{(B-2R)^2}{3A_m} \tag{B.4}$$

in which $k_V = 1.0$ for a continuous confinement, A_m is the cross-section area of the FRP confined member, and the confinement pressure f_l calculated as:

$$f_l = 2\frac{t_{FRP}E_{FRP}}{B}\varepsilon_{fd,rid} \tag{B.5}$$

where E_{FRP} and t_{FRP} are the Young's modulus and the FRP thickness, respectively; b and h are the cross-sectional dimensions and the ultimate strain for the FRP calculated as the minimum between:

$$\epsilon_{fd,rid} = \min\left\{\frac{\eta_a \epsilon_{fk}}{\gamma_f}; 0.004\right\} \tag{B.6}$$

here, it is assumed that $\eta_a = \gamma_f = 1.0$ and ϵ_{fk} is the characteristic value of the ultimate strain of the FRP, which is experimentally provided.

Appendix C. Literature data for the the hydrostatic compressive strength of mortar

In the works of *Hayen et al.* [42] it has been found that the hydrostatic compressive strength of mortar f'_{cm} can be found when:

$$\begin{cases} \text{Putty lime mortar:} & \sigma_1 \approx 2.66 f_{cm} \\ \text{Hydraulic lime mortar} & \sigma_1 \approx 3 f_{cm} \\ \text{Lime-cement mortar} & \sigma_1 \approx 2.92 f_{cm} \end{cases} \tag{C.1}$$

References

[1] Lourenço PB, Silva LC. Computational applications in masonry structures: from the meso-scale to the super-large/super-complex. International Journal for Multiscale Computational Engineering 2020;18(1):1–30. doi:10.1615/IntJMultCompEng.2020030889.

[2] Funari MF, Silva LC, Mousavian E, Lourenço PB. Real-time Structural Stability of Domes through Limit Analysis: Application to St. Peter's Dome. International Journal of Architectural Heritage 2021;:1–23doi:10.1080/15583058.2021.1992539.

[3] Funari MF, Silva LC, Savalle N, Lourenço PB. A concurrent micro/macro FE-model optimized with a limit analysis tool for the assessment of dry-joint masonry structures. International Journal for Multiscale Computational Engineering 2022;20(5):65–85. doi:10.1615/IntJMultCompEng.2021040212.

[4] European Committee for Standardization C. EN 1052-3: Methods of test for masonry–part 3: Determination of initial shear strength. 2007.

[5] Mojsilović N. Strength of masonry subjected to in-plane loading: A contribution. International Journal of Solids and Structures 2011;48(6):865–73. doi:10.1016/j.ijsolstr.2010.11.019.

[6] Hilsdorf HK. Investigation into the failure mechanism of brick masonry loaded in axial compression. Designing, engineering and constructing with masonry products. Gulf Publishing Company 1969;:34–41.

[7] Khoo C, Hendry A. A failure criterion for brickwork in axial compression. In: Proceeding of the 3rd International Brick/Block Masonry Conference. Essen, Germany; 1973, p. 139–45.

[8] Haseltine B. International rules for masonry and their effect on the UK. Masonry International 1987;1(2):41–3.

[9] Sarhat SR, Sherwood EG. The prediction of compressive strength of ungrouted hollow concrete block masonry. Construction and Building Materials 2014;58:111–21. doi:10.1016/j.conbuildmat.2014.01.025.

[10] ACI . ACI 530.1-02, Commentary on specification for masonry structures. Manual of concrete practice. Detroit, USA. 2004.

[11] EN 1996-1-1 . Eurocode 6: design of masonry structures. Part 1–1: general rules for reinforced and unreinforced masonry structures. 2005.

[12] McNary WS, Abrams DP. Mechanics of Masonry in Compression. Journal of Structural Engineering 1985;111(4):857–70. doi:10.1061/(ASCE)0733-9445(1985)111:4(857).

[13] Drougkas A, Roca P, Molins C. Compressive strength and elasticity of pure lime mortar masonry. Materials and Structures 2016;49(3):983–99. doi:10.1617/s11527-015-0553-2.

[14] Brencich A, Corradi C, Gambarotta L, Mantegazza G, Sterpi E. Compressive strength of solid clay brick masonry under eccentric loading. In: Proceeding of British Masonry Society. 2002, p. 37–46.

[15] Shrive NG, Jessop EL. An examination of the failure mechanism of masonry piers, prisms and walls subjected to compression. In: Proceeding of British Ceramic Society. 1982, p. 30–110.

[16] Lourenço PB, Pina-Henriques J. Validation of analytical and continuum numerical methods for estimating the compressive strength of masonry. Computers & Structures 2006;84(29):1977–89. doi:10.1016/j.compstruc.2006.08.009.

[17] Asteris PG, Argyropoulos I, Cavaleri L, Rodrigues H, Varum H, Thomas J, et al. Masonry Compressive Strength Prediction Using Artificial Neural Networks. Cham: Springer International Publishing. ISBN 978-3-030-12960-6; 2019, p. 200–24.

[18] Faella C, Martinelli E, Paciello S, Camorani G, Aiello MA, Micelli F, et al. Masonry columns confined by composite materials: Experimental investigation. Composites Part B: Engineering 2011;42(4):692–704. doi:10.1016/j.compositesb.2011.02.001.

[19] Corradi M, Grazini A, Borri A. Confinement of brick masonry columns with CFRP materials. Composites Science and Technology 2007;67(9):1772–83. doi:10.1016/j.compscitech.2006.11.002.

[20] Krevaikas TD, Triantafillou TC. Masonry Confinement with Fiber-Reinforced Polymers. Journal of Composites for Construction 2005;9(2):128–35. doi:10.1061/(ASCE)1090-0268(2005)9:2(128).

[21] Antonietta AM, Francesco M, Luca V. FRP Confinement of Square Masonry Columns. Journal of Composites for Construction 2009;13(2):148–58. doi:10.1061/(ASCE)1090-0268(2009)13:2(148).

[22] Pina-Henriques J, Lourenço PB. Masonry compression: a numerical investigation at the meso-level. Engineering Computations 2006;23(4):382–407. doi:10.1108/02644400610661163.

[23] Angelillo M, Lourenço PB, Milani G. Masonry behaviour and modelling. In: Angelillo M, editor. CISM International Centre for Mechanical Sciences, Courses and Lectures; vol. 551. ISBN 9783709117736; 2014, p. 1–26. doi:10.1007/978-3-7091-1774-3_1.

[24] Cascardi A, Aiello MA, Triantafillou T. Analysis-oriented model for concrete and masonry confined with fiber reinforced mortar. Materials and Structures 2017;50(4):202. doi:10.1617/s11527-017-1072-0.

[25] Witzany J, Čejka T, Zigler R. Failure mechanism of compressed short brick masonry columns confined with FRP strips. Construction and Building Materials 2014;63:180–8. doi:10.1016/j.conbuildmat.2014.04.041.

[26] Yuan Y, Milani G. Closed-form model for curved brittle substrates reinforced with FRP strips. Composite Structures 2023;304:116443. doi:10.1016/j.compstruct.2022.116443.

[27] Minafò G, D'Anna J, Cucchiara C, Monaco A, La Mendola L. Analytical stress-strain law of FRP confined masonry in compression: Literature review and design provisions. Composites Part B: Engineering 2017;115:160–9. doi:10.1016/j.compositesb.2016.10.019; composite lattices and multiscale innovative materials and structures.

[28] Grande E, Imbimbo M, Sacco E. Finite element analysis of masonry panels strengthened with FRPs. Composites Part B: Engineering 2013;45(1):1296–309. doi:10.1016/j.compositesb.2012.09.002.

[29] Grande E, Imbimbo M, Sacco E. Bond behaviour of CFRP laminates glued on clay bricks: Experimental and numerical study. Composites Part B: Engineering 2011;42(2):330–40. doi:10.1016/j.compositesb.2010.09.020.

[30] Triantafillou TC. Strengthening of masonry structures using epoxy-bonded FRP laminates. Journal of Composites for Construction 1998;2(2):96–104. doi:10.1061/(ASCE)1090-0268(1998)2:2(96).

[31] Di Ludovico M, D'Ambra C, Prota A, Manfredi G. FRP Confinement of Tuff and Clay Brick Columns: Experimental Study and Assessment of Analytical Models. Journal of Composites for Construction 2010;14(5):583–96. doi:10.1061/(ASCE)CC.1943-5614.0000113.

[32] Milani G. Simple model with in-parallel elasto-fragile trusses to characterize debonding on FRP-reinforced flat substrates. Composite Structures 2022;296:115874. doi:10.1016/j.compstruct.2022.115874.

[33] Napoli A, Realfonzo R. Compressive behavior of masonry columns confined with frcm systems: Research overview and analytical proposals. Journal of Composites for Construction 2022;26(3):04022019. doi:10.1061/(ASCE)CC.1943-5614.0001200.

[34] Pingaro N, Milani G. Simple non-linear numerical modelling of masonry arches reinforced with srg using elasto-fragile and elasto-ductile truss finite elements. Engineering Structures 2023;293:116637. doi:10.1016/j.engstruct.2023.116637.

[35] CNR-DT200 R1/2013 . Guide for design and construction of externally bonded FRP systems for strengthening existing structures: materials, RC and PC structures, masonry structures. 2013.

[36] Cascardi A, Longo F, Micelli F, Aiello MA. Compressive strength of confined column with fiber reinforced mortar (FRM): New design-oriented-models. Construction and Building Materials 2017;156:387–401. doi:10.1016/j.conbuildmat.2017.09.004.

[37] CNR-DT 212/2013 . Guide for the Probabilistic Assessment of the Seismic Safety of Existing Buildings. Tech. Rep.; National Research Council of Italy - Advisory Committee on Technical Recommendations for Construction; Rome; 2014.

[38] Aiello M, Bencardino F, Cascardi A, D'Antino T, Fagone M, Frana I, et al. Masonry columns confined with fabric reinforced cementitious matrix (FRCM) systems: A round robin test. Construction and Building Materials 2021;298:123816. doi:10.1016/j.conbuildmat.2021.123816.

[39] Thamboo J. Performance of masonry columns confined with composites under axial compression: A state-of-the-art review. Construction and Building Materials 2021;274:121791. doi:10.1016/j.conbuildmat.2020.121791.

[40] Lignola GP, Angiuli R, Prota A, Aiello MA. FRP confinement of masonry: analytical modeling. Materials and Structures 2014;47(12):2101–15. doi:10.1617/s11527-014-0323-6.

[41] Scacco J, Ghiassi B, Milani G, Lourenço PB. A fast modeling approach for numerical analysis of unreinforced and FRCM reinforced masonry walls under out-of-plane loading. Composites Part B: Engineering 2020;180(107553). doi:10.1016/j.compositesb.2019.107553.

[42] Hayen R, Van Balen K, Van Gemert D. The mechanical behavior of mortars in triaxial compression. Proceedings of the Arch Bridge IV-Advances in Assessment, Structural Design and Construction 2004;:395–404.

[43] Barbosa CS, Lourenço PB, Mohamad G, Hanai JB. Triaxial compression tests on bedding mortar samples looking at confinement effect analysis. In: 10th North American Masonry Conference. St. Louis, Missouri, USA; 2007, p. 1010–20.

[44] Hayen R, Van Balen K, Van Gemert D. Triaxial interaction of natural stone, brick and mortar in masonry constructions. Building Materials and Building Technology to Preserve the Built Heritage; Schueremans, L, Ed 2009;:333–52.

[45] Drougkas A, Roca P, Molins C. Analytical micro-modeling of masonry periodic unit cells – Elastic properties. International Journal of Solids and Structures 2015;69:169–88. doi:10.1016/j.ijsolstr.2015.04.039.

[46] Drougkas A, Verstrynge E, Hayen R, Van Balen K. The confinement of mortar in masonry under compression: Experimental data and micro-mechanical analysis. International Journal of Solids and Structures 2019;162:105–20. doi:10.1016/j.ijsolstr.2018.12.006.

[47] Mohamad G, Fonseca FS, Roman HR, Vermeltfoort AT, Rizzatti E. Behavior of mortar under multitaxial stress. In: Proceedings of the 12th

North American Masonry Conference, Denver. May; Denver, Colorado; 2015, p. 17–20.
[48] Vermeltfoort A, Martens D, Van Zijl G. Electronic speckle pattern interferometry observation of brick–mortar interface behaviour under compression. Canadian Journal of Civil Engineering 2007;34(11):1467–74. doi:10.1139/L07-070.
[49] Atkinson RH, Amadei BP, Saeb S, Sture S. Response of Masonry Bed Joints in Direct Shear. Journal of Structural Engineering 1989;115(9):2276–96. doi:10.1061/(ASCE)0733-9445(1989)115:9(2276).
[50] Tassios TP. Meccanica delle Murature. Napoli: Editore, Liguori; 1988.
[51] Mohamad G, Lourenço PB, Roman HR. Mechanics of hollow concrete block masonry prisms under compression: Review and prospects. Cement and Concrete Composites 2007;29(3):181–92. doi:10.1016/j.cemconcomp.2006.11.003.
[52] Ottosen NS. Constitutive model for short-time loading of concrete. Journal of the Engineering Mechanics Division 1979;105(1):127–41. doi:10.1061/JMCEA3.0002446.
[53] Rotunno T, Fagone M, Grande E, Milani G. Frcm-to-masonry bonding behaviour in the case of curved surfaces: Experimental investigation. Composite Structures 2023;313:116913. doi:10.1016/j.compstruct.2023.116913.
[54] Oliveira DV, Basilio I, Lourenço PB. Experimental bond behavior of FRP sheets glued on brick masonry. Journal of Composites for Construction 2011;15(1):32–41. doi:10.1061/(ASCE)CC.1943-5614.0000147.
[55] Ramirez R, Maljaee H, Ghiassi B, Lourenço PB, Oliveira DV. Bond behavior degradation between FRP and masonry under aggressive environmental conditions. Mechanics of Advanced Materials and Structures 2019;26(1):6–14. doi:10.1080/15376494.2018.1534164.
[56] Youssef MN, Feng MQ, Mosallam AS. Stress–strain model for concrete confined by FRP composites. Composites Part B: Engineering 2007;38(5):614–28. doi:10.1016/j.compositesb.2006.07.020; infrastructure Composites under Extreme Loadings.
[57] Lorenzis LD, Tepfers R. Comparative study of models on confinement of concrete cylinders with fiber-reinforced polymer composites. Journal of Composites for Construction 2003;7(3):219–37. doi:10.1061/(ASCE)1090-0268(2003)7:3(219).
[58] Han Q, Yuan W, Bai Y, Du X. Compressive behavior of large rupture strain (LRS) FRP-confined square concrete columns: experimental study and model evaluation. Materials and Structures 2020;53(4):99. doi:10.1617/s11527-020-01534-4.
[59] Sharma SS, Dave UV, Solanki H. FRP wrapping for rc columns with varying corner radii. Procedia Engineering 2013;51:220–9. doi:10.1016/j.proeng.2013.01.031; chemical, Civil and Mechanical Engineering Tracks of 3rd Nirma University International Conference on Engineering (NUiCONE2012).
[60] Gattuso C, Piccioli C, Gattuso P, Marra I, Tedesco A, Roviello V. A diagnostic plan for the cloister of Saint Augustine in Cosenza (Italy). In: Campanella L, Piccioli C, editors. 6th Conference on Diagnosis, Conservation and Valorization of Cultural Heritage. Naples, Italy: Edizioni AIES – Beni Culturali; 2015,.
[61] Olivito R, Tedesco A. Investigations about the structural damages of the cloister of St. Bernardino in Amantea (CS). In: Campanella L, Piccioli C, editors. 7th Conference on Diagnosis, Conservation and Valorization of Cultural Heritage. Naples, Italy: Edizioni AIES – Beni Culturali; 2016,.
[62] Tedesco A. Application of FRP materials on architectural elements in historical masonry. In: Campanella L, Piccioli C, editors. 8th Conference on Diagnosis, Conservation and Valorization of Cultural Heritage. Naples, Italy: Edizioni AIES – Beni Culturali; 2017,.
[63] Hilber HM, Hughes TJR, Taylor RL. Improved numerical dissipation for time integration algorithms in structural dynamics. Earthquake Engineering & Structural Dynamics 1977;5(3):283–92. doi:10.1002/eqe.4290050306.
[64] Szabó S, Funari MF, Lourenço PB. Masonry patterns' influence on the damage assessment of urm walls: Current and future trends. Developments in the Built Environment 2023;13:100119. doi:10.1016/j.dibe.2023.100119.
[65] Haller P. Hochhausbau in Backstein: die technischen Eigenschaften von Backstein-Mauerwerk für Hochhäuser. Orell Füssli; 1959.
[66] Yu W. An introduction to micromechanics. In: Composite Materials and Structures in Aerospace Engineering; vol. 828 of *Applied Mechanics and Materials*. Trans Tech Publications Ltd; 2016, p. 3–24. doi:10.4028/www.scientific.net/AMM.828.3.
[67] Voigt W. Ueber die beziehung zwischen den beiden elasticitätsconstanten isotroper körper. Annalen der Physik 1889;274(12):573–87. URL: https://onlinelibrary.wiley.com/doi/abs/10.1002/andp.18892741206. doi:https://doi.org/10.1002/andp.18892741206. arXiv:https://onlinelibrary.wiley.com/doi/pdf/10.1002/andp.18892741206.
[68] ACI 440.2R-02 . Guide for the Design and Construction of Externally Bonded FRP Systems for Strengthening Concrete Structures. American Concrete Institute; 2008. ISBN 9780870312854. doi:10.1061/40753(171)159.
[69] Lourenco PB, Gaetani A. Finite Element Analysis for Building Assessment: Advanced Use and Practical Recommendations. Taylor & Francis; 2022.
[70] FIB . fib Model Code for Concrete Structures 2010; chap. 5. John Wiley & Sons, Ltd. ISBN 9783433604090; 2013, p. 74–150. doi:https://doi.org/10.1002/9783433604090.ch5.
[71] Simo JC, Govindjee S. Exact closed-form solution of the return mapping algorithm in plane stress elasto-viscoplasticity. Engineering Computations 1988;5:254–8.
[72] Schreyer HL, Kulak RF, Kramer JM. Accurate Numerical Solutions for Elastic-Plastic Models. Journal of Pressure Vessel Technology 1979;101(3):226–34. doi:10.1115/1.3454627.
[73] Simo J. Numerical analysis and simulation of plasticity. In: Numerical Methods for Solids (Part 3) Numerical Methods for Fluids (Part 1); vol. 6 of *Handbook of Numerical Analysis*. Elsevier; 1998, p. 183–499. doi:10.1016/S1570-8659(98)80009-4.
[74] Armero F, Pérez-Foguet A. On the formulation of closest-point projection algorithms in elastoplasticity—part i: The variational structure. International Journal for Numerical Methods in Engineering 2002;53(2):297–329. doi:10.1002/nme.278.
[75] Sandoli A, Lignola GP, Calderoni B, Prota A. A design-oriented stress-strain constitutive model for clay-brick masonry columns confined by FRP. Key Engineering Materials 2022;916:147–54. doi:10.4028/p-653xvs.
[76] European committee for standardization (CEN) - Eurocode 6: Design of masonry structures – part 1: General rules for reinforced and unreinforced masonry structures. British Standard Institution London 2005;.
[77] ACI, ASCE, TMS, Commentary on specification for masonry structures. ACI5301-02/ASCE 6-02/TMS 602-02) 2004;.
[78] Atkinson R, Noland J, Abrams D. A deformation theory for stack bonded masonry prisms in compression. In: Proceedings of 7th International Brick Masonry Conference (Melbourne University, Melbourne, 1982). 1982, p. 565–76.